Coverage Performance in Multi-Stream MIMO-ZFBF Heterogeneous Networks

Mohammad G. Khoshkholgh, Kang G. Shin, *Life Fellow, IEEE*,
Keivan Navaie, *Senior Member, IEEE*, Victor C. M. Leung, *Fellow, IEEE*

***Abstract*— We study the coverage performance of multi-antenna (MIMO) communications in heterogenous networks (HetNets). Our main focus is on open-loop and multi-stream MIMO zero-forcing beamforming (ZFBF) at the receiver. Network coverage is evaluated adopting tools from stochastic geometry. Besides fixed-rate transmission (FRT), we also consider adaptive-rate transmission (ART) while its coverage performance, despite its high relevance, has so far been overlooked. On the other hand, while the focus of the existing literature has solely been on the evaluation of coverage probability per stream, we target coverage probability per communication link — comprising multiple streams — which is shown to be a more conclusive performance metric in multi-stream MIMO systems. This, however, renders various analytical complexities rooted in statistical dependency among streams in each link. Using a rigorous analysis, we provide closed-form bounds on the coverage performance for FRT and ART. These bounds explicitly capture impacts of various system parameters including densities of BSs, SIR thresholds, and multiplexing gains. Our analytical results are further shown to cover popular closed-loop MIMO systems, such as eigen-beamforming and space-division multiple access (SDMA). The accuracy of our analysis is confirmed by extensive simulations. The findings in this paper shed light on several important aspects of dense MIMO HetNets: (*i*) increasing the multiplexing gains yields lower coverage performance; (*ii*) densifying network by installing an excessive number of low-power femto BSs allows the growth of the multiplexing gain of high-power, low-density macro BSs without compromising the coverage performance; and (*iii*) for dense HetNets, the coverage probability does not increase with the increase of deployment densities.**

***Index Terms*— Coverage probability, densification, Heterogenous Cellular Networks (HetNets), Multiple-Input Multiple-Output (MIMO) systems, stochastic geometry, Poisson point process, Zero-Forcing Beamforming.**

I. Introduction

Multi-Input Multi-Output (MIMO) communication is a promising technology due to its potential of achieving high spectral efficiency and reliability often without requiring high transmission power [1]. Supported by decades of thorough investigations, MIMO communications have thus far been embodied in multiple IEEE 802.11 standards as well as 3GPP LTE-Advanced [2]. To cope with the rapid growth of wireless traffic demand [3], MIMO technologies have been re-emerging through copious innovative ideas. Thus, pervasive exploitations of sophisticated MIMO technologies in conjunction with unprecedented densification in heterogeneous networks (HetNets) are envisioned as the main design paradigm in next-generation cellular communication systems [4], [5].

There has been extensive research on the application of MIMO in HetNets, mainly focusing on isolated scenarios (e.g., [6]); for example, by evaluating the performance of femto-cells overlaying/underlaying macro-cells. This line of research, however, falls short of characterizing the network-wise performance of MIMO in HetNets. Network-wise performance is of utmost importance when it comes to design and implementation of large-scale communication systems with millions of nodes. This shortcoming is rooted in the simplified and often unrealistic assumptions made on the incorporation of inter-cell interference (ICI) in system analysis. As a result, while in a single cell system, allocating the system resources is rather straightforward, the same cannot be directly applied in the network-wise performance context. For instance, in a single cell system, decisions such as the number of antennas to be switched on/off, the number of user equipments (UEs) to be concurrently served, or choosing between multiplexing (using antennas for increasing data rate) and diversity (using antennas for increasing reliability) are easy to make [1], [7], whereas in a multi-cell network, such decisions need sophisticated solutions incorporating the inter-cell impact based on network-wise performance metrics. While increasing the number of transmitted data streams (i.e., increasing the multiplexing gain) in a single-cell system is (locally) optimal, it increases the ICI, almost with the same order, which could offset the effect of the former. It is, therefore, debatable whether strategies yielding higher capacity or better coverage from the perspective of local decisions (isolated scenarios) result in network-wise optimality.

One approach to capturing the network-wise effects of adopting MIMO is to employ analytical tools from stochastic geometry, see, e.g., [8], [9] and references therein. Such techniques are widely used in modeling and analyzing ad hoc and sensor networks, [10], [11], [12], and recently cellular communications [13]. Some researchers, however, have casted skepticism on the accuracy of Poisson Point Process (PPP) for modeling the locations of macro BSs [14]. This is because PPP models position the BSs in the network plane almost indiscriminately, whereas in practice, macro BSs are often placed far from each other. This issue is investigated further in [13], where the PPP assumption is shown to result in adequately

Manuscript received April 29, 2016, revised September 13, 2016.

M. G. Khoshkholgh and V. C. M. Leung (m.g.khoshkholgh@gmail.com, vleung@ece.ubc.ca) are with the Department of Electrical and Computer Engineering, the University of British Columbia, Vancouver, BC, Canada V6T 1Z4 ; K. G. Shin (kgshin@umich.edu) is with the Department of Electrical Engineering and Computer Science, University of Michigan, Ann Arbor, MI 48109-2121, U.S.A.; K. Navaie (k.navaie@lancaster.ac.uk) is with School of Computing and Communications, Lancaster University, Bailrigg Lancaster LA1 4WA United Kingdom.

precise characterization of macro BSs, and in fact, provides a rather pessimistic bound on the coverage performance in contrast to other analytic methods such as hexagonal and lattice models, see, e.g., [15] that provide optimistic bounds. The PPP models have also been widely used for modeling and analyzing HetNets, e.g., [16], [17], [18]. The pioneering work of [16] proposed a flexible approach in modeling K-tier HetNets[1] through K tiers of independent PPPs.

In this paper, we extend the approach in [16] to multi-stream MIMO HetNets and investigate their coverage performance. Our focus is on open-loop MIMO zero-forcing beamforming (MIMO-ZFBF), which is practically attractive due to its straightforward implementation, low computational complexity, and almost zero feedback overhead. The network-wise performance of MIMO-ZFBF, as well as other pertinent MIMO techniques, is nevertheless extensively studied in the context of ad hoc networks, see, e.g., [19], [20], [21], [22], [23], [24]. The work of [20] is practically relevant to this paper as their focus is also on open loop MIMO such as ZFBF. Several advantages of ZFBF in enhancing the coverage performance of ad hoc networks were highlighted there, and multi-stream communications were proven to outperform ideal single-stream ad hoc networks for practical settings.

In light of the above findings in the context of ad hoc networks, one may argue that the same trends can hold in MIMO HetNets by noticing the convergence, albeit partial, of HetNets toward ad hoc networks, for instance through *random* installation of remote antenna ports, relays, and small cells. Apart from such analogies, there exist significant discrepancies between these two networks due mainly to the corresponding CA mechanisms governing HetNets, as well as centralized TDMA/FDMA MAC protocols.

It is, therefore, necessary to investigate *whether or not multi-stream MIMO schemes are of practical significance in enhancing the coverage performance of HetNets?* It is equally important to understand *whether in MIMO HetNets, cell densification and high multiplexing gains should be practiced simultaneously in all tiers?* If not, *new techniques are needed to evaluate whether for a given setting excessive densification is preferable to increasing multiplexing gains?*

Despite significant progress in analyzing MIMO communications in HetNets, the existing results are inadequate to comprehensively address the above concerns and other similar questions. To address this inadequacy, we derive closed-form bounds on the the coverage performance of MIMO communications. The thus-obtained analytical results enable thorough investigation of densification and multiplexing gains in MIMO HetNets.

A. Related Work

The authors of [25] considered MIMO-based HetNets where a single macro-cell system overlaid by a number of multi-antenna femto cells was investigated. The system in [25] adopts spatial division multiple access (SDMA) beamforming and in each cell, a number of UEs, each with a single antenna, are served. For this configuration, the authors of [25] show that the system achieves a higher area spectral efficiency by solely serving one UE per femto-cell via conventional beamforming. The results in [25] are extended in [26] to K-tier multi-input single-output (MISO) HetNets, under the assumption of maximum SIR CA rule. By comparing the coverage probability, the authors of [26] showed that spatial division multiple access (SDMA) is inferior to the schemes which support one UE per cell. This conclusion is also confirmed in [27] for a clustered ad hoc network with quantized beamforming.

Area spectral efficiency of MISO-SDMA systems is studied in [28], [29] assuming *range expansion* CA rule, where UEs are associated with the BS with the smallest path-loss. The authors of [28], [29] then provide algorithms for optimizing the system spectral efficiency. A number of approaches have been outlined in [30] paving the way of effective construction of scales in range expansion for MISO-SDMA systems. The bit-error probability of zero-forcing (ZF) precoding with the aid of modeling ICI through a properly fitted Gaussian distribution is derived in [31]. The authors of [32], [33] studied the outage performance of different receiver techniques with the range expansion method as the association rule.

The post-processing SIR in MIMO communications often involves Nakagami-fading type fluctuations. In this regard, the studies in [34] and [35] are closely related to this paper. The authors of [34] provided results on the coverage probability of optimal combining receiver under Nakagami fading channels in ad hoc networks, which are not directly extendable to the cellular systems. Furthermore, an analytical framework is developed in [35] by which various functions of interference processes in Poisson network can be characterized. The authors of [35] also derived the outage probability in a system with Nakagami-fading in ad hoc networks.

Open-loop orthogonal space-time codes are the focus of analysis in [32], where only one multi-antenna UE is considered per cell. In their analysis, two receiver techniques are considered based on canceling and ignoring the ICI. Formulas for the probability of coverage are provided for both cases in [32]. Focusing on single tier systems, minimum mean square estimation (MMSE) and partial zero forcing (PZF) beamforming schemes are then investigated in [33], where both MMSE and PZF are shown to be effective in canceling dominant interferers.

B. Main Contributions and Organization of the Paper

Unlike the existing MIMO HetNets which mainly focus on range expansion (see, e.g., [28], [30], [32], [33]), we focus on CA rule based on the strongest instantaneous received power as in [16], [26]. It is important to note that the CA rules in [28], [32], [33] are equivalent to their counterpart in single-antenna regimes, see, e.g., [13], [18], [36], and thus overlook the key MIMO characteristics including multiplexing and diversity in the CA stage. Such limitations are alleviated when the instantaneous received power is considered as the value of SIR explicitly and accurately captures the interplays existing among diversity, multiplexing, and ICI in MIMO communications. Extension of this rule to multi-stream MIMO is however non-trivial, since *UEs should stay associated with*

[1] K-tier HetNets consist of K spatially and spectrally coexisting tiers, each with its own BS.

the same BS on all the streams. In this paper, we also introduce analytical techniques that effectively deal with these requirements.

In existing ad hoc networks and MIMO HetNets, only fixed-rate transmission (FRT) is considered. This is inadequate to analyze HetNets where BSs can adaptively schedule data among the streams. To the best of our knowledge, the network-wise performance of adaptive-rate transmission (ART) is investigated in this paper for the first time. To analyze ART, the statistics of the aggregated scheduled data rate on the streams is required in which mathematical tractability is a challenging task which we address in this paper.

Note, also, that while only the *coverage probability per data stream* has been studied in the related literature, here we evaluate the *coverage probability per communication link* running multiple streams. From an analytical viewpoint, the streams' SIR in a communication link are statistically dependent. Therefore, (*i*) the existing results of dealing with the former metric are not generally extensible for studying the performance of FRT and ART, (*ii*) the analytical evaluation of the latter metric is much more complicated than the former, and (*iii*) the former is unable to provide the whole picture of the performance of MIMO communications. Our results indicate that by varying system parameters, there are significant discrepancies between these two metrics.

Finally, the coverage probability bounds provided in [22], [26], [28], [29], [30], [32], [33] do not clearly interpret the impact of system parameters on the coverage performance, and also require calculation of high-order derivatives of the ICI Laplace transform which adds further analytical complications. One distinct feature of our approach is the derivation of an analytical bound on the coverage probability that provides quantitative insight in the impact of key system parameters on the FRT and ART performance. In particular, our findings suggest that: (*i*) As a rule of thumb, increasing multiplexing gains reduces the coverage performance, particularly when the network is sparse, i.e., low density of the BSs. (*ii*) For dense networks where BSs are densely populated in the coverage area, there exist scenarios in which increasing the density of BSs as well as the multiplexing gains does not degrade the coverage performance. In fact, if densification is practiced in low-power tiers, it allows the growth of the multiplexing gains of high-power low-density macro BSs, without compromising the coverage performance. In particular, this finding has a significant economical significance in designing cost-effective HetNets in the evolution phase. (*iii*) The ART coverage performance is much higher than that of FRT's, while its signaling overhead is manageable. This is an important practical finding as a significant coverage performance can be achieved with a low signaling overhead and simple transmitters/receivers, e.g., open-loop ZFBF, without any need to acquire channel matrices. This is import in ultra dense networks which are vulnerable to feedback overhead, pilot contamination, and complexity of the MIMO techniques.

Although our main focus is on the open-loop ZFBF, we will later extend our analysis to some important closed-loop cases such as eigen-beamforming (i.e., maximum ratio transmission (MRT)) and MISO-SDMA with ZFBF at the transmitters, where analytical results on their associated coverage performance are in general unavailable [26].

The rest of this paper is organized as follows. The system model and main assumptions are presented in Section II. Coverage performances of FRT and ART are then analyzed in Section IV. We then present an extension of analysis to several important MIMO scenarios in Section V followed by numerical analysis and simulation results in Section VI. The paper is concluded in Section VII.

II. System Model

Consider downlink communication in heterogeneous cellular networks (HetNets) comprising $K \geq 1$ tiers of randomly located BSs. The BSs of tier $i \in \mathcal{K}$ are spatially distributed according to a homogenous Poisson Point Process (PPP), Φ_i, with spatial density, $\lambda_i \geq 0$, where λ_i is the number of BSs per unit area [16]. We further assume that Φ_i, $i \in \mathcal{K}$ are mutually independent.

In this model, each tier i is fully characterized by the corresponding spatial density of BSs, λ_i, their transmission power, P_i, the SIR threshold, $\beta_i \geq 1$, the number of BSs' transmit antennas, N_i^t, and the number of scheduled streams $S_i \leq \min\{N_i^t, N^r\}$ (also referred to as *multiplexing gain*), where N^r is the number of antennas in the user equipments (UEs). Here, the modeled system of multi-stream data communication is considered as S_i pipes of information [21], [20]. UEs are also randomly scattered across the network and form a PPP, Φ_U, independent of $\{\Phi_i\}$s, with density, λ_U. In the system the time is slotted and similar to [25], [26], [27], [32]. Our focus is on the scenarios in which at each given time slot only one UE is served per active cell. In cases where more than one UE is associated with a given BS, time-sharing is adopted for scheduling.

Our main objective in this paper is to evaluate the network coverage performance. According to Slivnayak's Theorem [8], [9] and due to the stationarity of the point processes, the spatial performance of the network can be adequately obtained from the perspective of a *typical UE* virtually positioned at the origin. The measured performance then attains the spatial representation of the network performance, thus the same performance is expected throughout the network.

Let a typical UE be associated with BS x_i transmitting S_i data streams. Ignoring the impact of background noise,[2] the received signal, $\boldsymbol{y}_{x_i} \in \mathbb{C}^{N^r \times 1}$ ($\mathbb{C}$ is the set of complex numbers), is

$$\boldsymbol{y}_{x_i} = \|x_i\|^{-\frac{\alpha}{2}} \boldsymbol{H}_{x_i} \boldsymbol{s}_{x_i} + \sum_{j \in \mathcal{K}} \sum_{x_j \in \Phi_j / x_0} \|x_j\|^{-\frac{\alpha}{2}} \boldsymbol{H}_{x_j} \boldsymbol{s}_{x_j}, \quad (1)$$

where $\forall x_i, i \in \mathcal{K}$, $\boldsymbol{s}_{x_i} = [s_{x_i,1} \dots s_{x_i,S_i}]^T \in \mathbb{C}^{S_i \times 1}$, $s_{x_i,l} \sim \mathcal{CN}(0, P_i/S_i)$ is the transmitted signal corresponding to stream l in tier i, $\boldsymbol{H}_{x_i} \in \mathbb{C}^{N^r \times S_i}$ is the fading channel matrix between BS x_i and the typical UE with entries independently drawn from $\mathcal{CN}(0,1)$, i.e., Rayleigh fading assumption. Transmitted signals are independent of the channel matrices. In (1), $\|x_i\|^{-\alpha}$ is the distance-dependent path-loss attenuation, where $\|x_i\|$ is the Euclidian distance between BS x_i and the origin, and $\alpha > 2$ is the path-loss exponent. We define

[2] **In practice, HetNets with universal frequency reuse are interference-limited, and the thermal noise is thus much smaller than the interference and it is often ignorable.**

$\breve{\alpha} = 2/\alpha$ and assume perfect CSI at the UEs' receiver (CSIR), $\boldsymbol{H}_{x_i}$.

We focus on the scenarios in which the channel state information at the transmitter (CSIT) is unavailable, and hence the BSs of each tier i simply turn on S_i transmit antennas where the transmit power P_i is equally divided among the transmitted data streams. Such simple pre-coding schemes are often categorized as *open-loop* techniques, see, e.g., [20], [21]. Although open-loop techniques are not necessarily capable of full exploitation of the available degrees-of-freedom (DoF),[3] they are practically appealing. This is partly due to the simplicity of the BSs' physical layer configuration (especially low-power BSs, such as femto-cells and distributed antenna ports) in which CSIT is not required, and partly because of the simple and straightforward UE structure. Note that availability of the CSIT further imposes a high signaling overhead in ultra-dense HetNets with universal frequency reuse which is practically challenging [20], [21], [32].

The practical importance of open-loop techniques makes it critical to inspect the network-wise performance of such techniques. In this paper, we analyze a dominant open-loop technique *viz.* zero-forcing beamforming (ZFBF) at the receiver [20]. In addition to its practical simplicity, ZFBF provides mathematical tractability, which is hard to achieve in most of the MIMO-based techniques.

Adopting ZF, a typical UE utilizes the CSIR, $\boldsymbol{H}_{x_i}$, to mitigate the inter-stream interference. The cost is however reducing DoF per data stream. Therefore, to decode the l_i-th stream, the typical UE obtains matrix $(\boldsymbol{H}_{x_i}^{\dagger}\boldsymbol{H}_{x_i})^{-1}\boldsymbol{H}_{x_i}^{\dagger}$, where $\dagger$ is the conjugate transpose, and then multiplies the conjugate of the l_i-th column by the received signal in (1). Let intending channel power gains[4] associated with the l_i-th data stream, $H^{\mathrm{ZF}}_{x_i,l_i}$, and the ICI caused by $x_j \neq x_i$ on data stream l_i, $G^{\mathrm{ZF}}_{x_j,l_i}$, be Chi-Squared random variables with DoF of $2(N^r - S_i + 1)$, and $2S_j$, respectively. Using the results of ([20] Section II-A, Eq. (7)), the SIR associated with the l_i-th stream is

$$\mathrm{SIR}^{\mathrm{ZF}}_{x_i,l_i} = \frac{\frac{P_i}{S_i}\|x_i\|^{-\alpha} H^{\mathrm{ZF}}_{x_i,l_i}}{\sum\limits_{j\in\mathcal{K}}\sum\limits_{x_j\in\Phi_j/x_i}\frac{P_j}{S_j}\|x_j\|^{-\alpha} G^{\mathrm{ZF}}_{x_j,l_i}}. \tag{2}$$

Note that for each l_i, $H^{\mathrm{ZF}}_{x_i,l_i}$ and $G^{\mathrm{ZF}}_{x_j,l_i}$ are independent random variables (r.v.)s. Further, $H^{\mathrm{ZF}}_{x_i,l_i}$ ($G^{\mathrm{ZF}}_{x_j,l_i}$) and $H^{\mathrm{ZF}}_{x_i,l}$ ($G^{\mathrm{ZF}}_{x_j,l}$) are independent and identically distributed (i.i.d.) for $l \neq l_i$. In (2), for a given communication link, $\mathrm{SIR}^{\mathrm{ZF}}_{x_i,l_i}$, are identically, but not independently, distributed across streams. Finally, because of path-loss attenuations the SIR values among the streams in (2) are statistically dependent.

As shown in (2), increasing S_i has conflicting impacts on the SIR. It reduces the per-stream intended DoF as well as per-stream power which results in reduction of the received power of both intended and interfering signals. Increasing S_i also increases the DoF of the ICI fading channels. To understand the relationship between the multiplexing gains on the network coverage performance (the exact definition of network coverage performance is provided in Section III), in the rest of this paper we investigate the statistics of $\mathrm{SIR}^{\mathrm{ZF}}_{x_i,l_i}$.

[3]DoF of a MIMO channel is the number of independent streams of information that can be reliably transmitted simultaneously.

[4]Hereby the term "intending" is used to describe the characteristics of the channel between the typical UE and its serving BS.

III. Coverage Probability in Multi-Stream MIMO Cellular Communications

In the literature of multi-stream MIMO communications both in ad hoc (see, e.g., [20], [21], [22], [37], [24]), and cellular networks (see, e.g., [32]), the *coverage probability per stream* is considered as the main performance metric. Accordingly, if $\mathrm{SIR}^{\mathrm{ZF}}_{x_i,l_i} \geq \beta_i$, the typical UE is then able to accurately detect the l_i-th stream of data, and thus is in the coverage area. Note that coverage probability per stream is the probability of event $\{\mathrm{SIR}^{\mathrm{ZF}}_{x_i,l_i} \geq \beta_i\}$. To understand it, it is then only required to investigate the statistical characteristics of $\mathrm{SIR}^{\mathrm{ZF}}_{x_i,l_i}$.

However, there are at least two main issues related to this performance metric. First, it is not practically extendible to cellular systems due mainly to CA mechanism. In fact, the mathematical presentation of the multi-stream MIMO communications involves S_i different SIR expressions on each tier i, see, (2). The analytical model of "coverage probability per stream" may rise scenarios that the typical UE receives data from different BSs on different streams. But in practice, the typical UE receives S_i streams of data from merely a single BS. Second, the coverage performance of the communication link comprising of S_i streams can not be accurately predicted by the performance on a given stream. This is because SIR values among streams are correlated, which as reported in [38] (although for the case of SIMO ad hoc networks) results in severe reduction of the diversity of multi-antenna arrays. In our view this correlation can further affect the multiplexing gain of the multi-stream MIMO HetNets too, which its ramifications on the coverage performance of the system has to be understood.

As a result, the considered definition of coverage probability in the literature of multi-stream MIMO is not appropriate for cellular systems. To make the analytical model consistent with the reality of cellular systems we then require to define a new, and thus more comprehensive, definition of the coverage probability. To this end, here we consider the *coverage probability per communication link*[5] as the main performance metric. The exact definition of this new metric is however contingent the transmission strategy that BSs are practicing.

A. Transmission Strategies at the BSs

As mentioned above, the characteristics of the coverage performance in MIMO HetNets depends on the adopted transmission strategy at the BSs. BSs adopt either *fixed-rate transmission* (FRT) or adaptive-rate transmission (ART) schemes, where for the latter UEs need to feed back the achievable capacity per streams. In the FRT scheme the transmission rate on each stream, l_i, in the typical UE which is associated to BS x_i is constant and equal to $R_{x_i,l_i} = \log(1+\beta_i)$ nat/sec/Hz, where β_i is corresponding SIR threshold. Thus, the total received data rate is $R_{x_i} = S_i \log(1+\beta_i)$. On the other hand, in ART scheme the total transmission rate across S_i streams is equal to $R_{x_i} = \sum\limits_{l_i=1}^{S_i} \log(1+\mathrm{SIR}_{x_i,l_i})$ symbol/sec/Hz.

[5]In this paper we commonly refer to "the coverage probability per link" as "the coverage performance," unless otherwise stated.

B. Coverage Probability in Multi-Stream MIMO Systems

We now specify the CA mechanism in both cases of FRT and ART schemes so that the typical UE stays associated with a single BS across all streams. For the case of FRT scheme, the typical UE is associate to the BS in which the weakest[6] SIR across the streams is larger than the corresponding SIR threshold, β_i. In the other words for all S_i scheduled streams the corresponding SIR values must satisfy the required SIR threshold. Accordingly, the typical UE is considered in the coverage area if $\mathcal{A}_{\text{FRT}}$ is nonempty, where

$$\mathcal{A}_{\text{FRT}} = \left\{ \exists i \in \mathcal{K} : \max_{x_i \in \Phi_i} \min_{l_i=1,\ldots,S_i} \text{SIR}_{x_i,l_i} \geq \beta_i \right\}. \quad (3)$$

For the case of ART scheme, the typical UE is considered in the coverage area if $\mathcal{A}_{\text{ART}}$ is nonempty, where $\mathcal{A}_{\text{ART}} =$

$$\left\{ \exists i \in \mathcal{K} : \max_{x_i \in \Phi_i} \sum_{l_i=1}^{S_i} \log\left(1+\text{SIR}_{x_i,l_i}\right) \geq S_i \log(1+\beta_i) \right\}. \quad (4)$$

Note that to preserve consistency between FRT and ART schemes, we set the required transmission rate in the ART scheme equal to $S_i \log(1+\beta_i)$.

The FRT scheme is more suitable for the MIMO transceiver structures that the symbol error rate (SER) is mainly influenced by the statistics of the weakest data stream, while the ART scheme is closely related to the spatially coded multiplexing systems [1]. One may thus consider a combination of FRT and ART schemes in an adaptive mode selection scheme in applications such as device-to-device (D2D) and two-hop cellular communications. For instance, if the cellular system is lightly-loaded, then by adopting the ART, it is possible to serve many new devices by the single-hop cellular communications. On the other hand, when the system is heavily-loaded, part of the load can be adaptively offloaded to proximity-aware D2D communications by switching to the FRT scheme.

Having defined the transmission strategies, CA mechanisms, and coverage per link, we can now analyze the coverage performance of MIMO HetNets.

IV. Analyzing the Coverage Performance

A. The FRT Scheme

Proposition 1: The coverage probability of the FRT-ZFBF scheme, $O_{\text{FRT}}^{\text{ZF}}$, is upper-bounded as

$$O_{\text{FRT}}^{\text{ZF}} \leq \frac{\pi}{\tilde{C}(\alpha)} \sum_{i \in \mathcal{K}} \frac{\lambda_i \left(\frac{P_i}{S_i^2 \beta_i}\right)^{\check{\alpha}} \left(\sum_{m_i=0}^{N^r-S_i} \frac{\Gamma(\frac{\check{\alpha}}{S_i}+m_i)}{\Gamma(\frac{\check{\alpha}}{S_i})\Gamma(1+m_i)} \right)^{S_i}}{\sum_{j \in \mathcal{K}} \lambda_j \left(\frac{P_j}{S_j}\right)^{\check{\alpha}} \left(\frac{\Gamma(\frac{\check{\alpha}}{S_i}+S_j)}{\Gamma(S_j)}\right)^{S_i}}, \quad (5)$$

where $\tilde{C}(\alpha) = \pi\Gamma(1-\check{\alpha})$, and $\Gamma(.)$ is the gamma function.

Proof: See Appendix A. □

The bound presented in Proposition 1 reflects the effect of system parameters including multiplexing gains, S_is, deployment densities, λ_i, and transmission powers, P_i, on the the coverage performance. Using Proposition 1, the coverage performance for tier i is upper-bounded as

$$O_{\text{FRT},i}^{\text{ZF}} \leq \frac{\frac{\pi\lambda_i}{\tilde{C}(\alpha)} \left(\frac{P_i}{S_i}\right)^{\check{\alpha}} \beta_i^{-\check{\alpha}} S_i^{-\check{\alpha}} \left(\sum_{m_i=0}^{N^r-S_i} \frac{\Gamma(\frac{\check{\alpha}}{S_i}+m_i)}{\Gamma(\frac{\check{\alpha}}{S_i})\Gamma(1+m_i)} \right)^{S_i}}{\sum_{j \in \mathcal{K}} \lambda_j \left(\frac{P_j}{S_j}\right)^{\check{\alpha}} \left(\frac{\Gamma(\frac{\check{\alpha}}{S_i}+S_j)}{\Gamma(S_j)}\right)^{S_i}}. \quad (6)$$

[6]From practical viewpoint such requirement is necessary as it allows the incorporation of this fact that all the streams of data are originated from a unique BS.

Based on the bound in (6), we make the following observations:

1)In (6), increasing multiplexing gains, S_i reduces per-stream power in both numerator and denominator, which is indicative of the intended signals through the term, $\left(\frac{P_i}{S_i^2\beta_i}\right)^{\check{\alpha}}$, and ICI, via term $\left(\frac{P_j}{S_j}\right)^{\check{\alpha}}$, $\forall j \in \mathcal{K}$. Note that the BSs in each tier also interfere each other.

2) S_i has an impact on the level of ICI imposed from tiers $j \neq i$ (through $\left(\frac{\Gamma(\frac{\check{\alpha}}{S_i}+S_j)}{\Gamma(S_j)}\right)^{S_i} \geq 1$), and from BSs in tier i (through $\left(\frac{\Gamma(\frac{\check{\alpha}}{S_i}+S_i)}{\Gamma(S_i)}\right)^{S_i} \geq 1$), both increasing functions of S_i. Therefore, the impact of ICI is increased by fixing the multiplexing gains in all BSs across all tiers and increasing the multiplexing gain in a particular cell. Therefore, policies such as ZFBF at the receivers enforcing reluctance toward systematically dealing with ICI—by canceling some strong interferers, for instance—has unexpected impact on the growth of the ICI due to the home cell multiplexing gain.[7] In other words, when dealing with multi-stream transmission, the exact representation of ICI can be magnified via the practiced multiplexing gain at the home cell, irrespective of the multiplexing gains in the adjacent cells. By considering per-stream coverage probability as the performance metric (see, e.g., [21], [22], [32]), and following the same lines of arguments in the proof of Proposition 1, one can also show that the coverage probability per stream l_i is[8]

$$O_{\text{FRT},i,l_i}^{\text{ZF}} \leq \frac{\pi}{\tilde{C}(\alpha)} \frac{\lambda_i \left(\frac{P_i}{S_i}\right)^{\check{\alpha}} \beta_i^{-\check{\alpha}} \sum_{m_i=0}^{N^r-S_i} \frac{\Gamma(\check{\alpha}+m_i)}{\Gamma(\check{\alpha})\Gamma(1+m_i)}}{\sum_{j \in \mathcal{K}} \lambda_j \left(\frac{P_j}{S_j}\right)^{\check{\alpha}} \frac{\Gamma(\check{\alpha}+S_j)}{\Gamma(S_j)}}. \quad (7)$$

In the upper-bound, the effect of the ICI imposed from tier $j \neq i$ is shown to be represented solely through $\frac{\Gamma(\check{\alpha}+S_j)}{\Gamma(S_j)}$ which is independent of S_i. Since $\frac{\Gamma(\frac{\check{\alpha}}{S_i}+S_j)}{\Gamma(S_j)} \leq \frac{\Gamma(\check{\alpha}+S_j)}{\Gamma(S_j)}$, multiplexing gain S_i could reduce the negative effect of higher multiplexing gain S_j, on the link performance compared to the given stream performance due to the dependency of SIR values among the streams. *A direct conclusion is that performance of a given stream of a communication link does not necessarily represent the entire picture of the communication link performance.*

3) The multiplexing gain S_i affects the intended signal strength in (6) via $S_i^{-\check{\alpha}} \left(\sum_{r_i=0}^{N^r-S_i} \frac{\Gamma(\frac{\check{\alpha}}{S_i}+r_i)}{\Gamma(\frac{\check{\alpha}}{S_i})\Gamma(1+r_i)} \right)^{S_i}$ that is dependent on N^r-S_i+1 which is the available DoF for transmitting each stream of data. Comparing (6) with (7), one can see that by considering the per-stream coverage as the performance metric, this effect is overlooked.

For $\beta_i = \beta$ and $S_i = S$, $\forall i$, (5) is reduced to

$$O_{\text{FRT}}^{\text{ZF}} \leq \frac{\pi S^{-\check{\alpha}}}{\tilde{C}(\alpha)} \left(\frac{\Gamma(S)}{\Gamma(\frac{\check{\alpha}}{S}+S)} \sum_{m=0}^{N^r-S} \frac{\Gamma(\frac{\check{\alpha}}{S}+m)}{\Gamma(\frac{\check{\alpha}}{S})\Gamma(1+m)} \right)^{S}, \quad (8)$$

[7]Analytical results in this paper do not necessarily suggest the same for the MMSE-based and closed-loop MIMO techniques, as well as techniques that force cancellation of dominant interferers.

[8]Such an expression for the coverage probability per stream does not exist in the literature except for high SNR regimes as in [29].

that demonstrates scale-invariance, i.e., the coverage probability does not change with the changes in the density of the deployment of BSs.

B. The ART Scheme

Here we focus on the ART scheme. According to Campbell-Mecke's Theorem [8], [9], the corresponding coverage probability is $O_{\rm ART}^{\rm ZF} \leq$

$$\sum_{i\in\mathcal{K}} 2\pi\lambda_i \int_0^{\infty} r_i \mathbb{P}\left\{\sum_{l_i=1}^{S_i} \log\left(1+\mathrm{SIR}_{x_i,l_i}\right) \geq S_i \log(1+\beta_i)\right\} \mathrm{d}r_i. \tag{9}$$

Analyzing (9) is, however, challenging due to the complexity of obtaining probability distribution function of $\sum_{l_i=1}^{S_i} \log(1+\mathrm{SIR}_{x_i,l_i})$. Utilizing Markov's inequality results in the following bound (see Appendix B in the supplementary document)

$$O_{\rm ART}^{\rm ZF} \leq \frac{\alpha}{2} \sum_{i\in\mathcal{K}} \frac{\frac{\lambda_i}{\log(1+\beta_i)} \left(\frac{P_i}{S_i}\right)^{\check{\alpha}} \frac{\Gamma(\check{\alpha}+N_i^t-S_i+1)}{\Gamma(N_i^t-S_i+1)}}{\sum_{j\in\mathcal{K}} \lambda_j \left(\frac{P_j}{S_j}\right)^{\check{\alpha}} \frac{\Gamma(\check{\alpha}+S_j)}{\Gamma(S_j)}}. \tag{10}$$

However, the upper-bound in (10) is loose. So, in Proposition 2 we derive a tighter upper-bound using a heuristic approximation and based on the FRT coverage bound, $O_{\rm FRT}^{\rm ZF}$.

Proposition 2: The coverage probability of the ART-ZFBF scheme, $O_{\rm ART}^{\rm ZF}$, is approximated as

$$O_{\rm ART}^{\rm ZF} \lessapprox 0.5 O_{\rm FRT}^{\rm ZF} + 0.5 \frac{\pi}{\tilde{C}(\alpha)} \sum_{i\in\mathcal{K}} \sum_{l_i=1}^{S_i} \binom{S_i}{l_i} (-1)^{l_i+1}$$

$$\frac{\frac{\lambda_i}{l_i^{\check{\alpha}}} \left(\frac{P_i}{S_i\beta_i}\right)^{\check{\alpha}} \left(\sum_{m_i=0}^{N^r-S_i} \frac{\Gamma(\frac{\check{\alpha}}{l_i}+m_i)}{\Gamma(\frac{\check{\alpha}}{l_i})\Gamma(1+m_i)}\right)^{l_i}}{\sum_{j\in\mathcal{K}} \lambda_j \left(\frac{P_j}{S_j}\right)^{\check{\alpha}} \left(\frac{\Gamma(\frac{\check{\alpha}}{l_i}+S_j)}{\Gamma(S_j)}\right)^{l_i}}, \tag{11}$$

where $O_{\rm FRT}^{\rm ZF}$ is given in Proposition 1.

Proof: See Appendix C. □

The impacts of multiplexing gains, S_is, deployment densities, λ_i, and transmission powers, P_i, on the the coverage performance are evident in (11). Similar to the FRT scheme, for $\beta_i = \beta$ and $S_i = S, \forall i$, (11) demonstrates scale-invariance.

Note that since $\mathcal{A}_{\rm FRT} \subseteq \mathcal{A}_{\rm ART}$ there holds $O_{\rm ART}^{\rm ZF} \geq O_{\rm FRT}^{\rm ZF}$. Later in Section VI, we will present numerical results of comparing the outage probability of the FRT and ART schemes.

V. Extensions of the Analysis

As mentioned before, the main focus of this paper is on the evaluation of coverage performance in open-loop ZFBF systems. However, the analysis is general enough to predict the coverage performance of other practically relevant HetNets. In this section we provide various examples of showing how the derived analytical results in Section IV can be employed to predict the coverage probability of other HetNets. For simplicity, here we only consider the FRT scheme.

A. Single-Input Single-Output (SISO) Systems

The results presented in Section IV can be fit to the SISO systems by simply setting $S_i = N_i^t = N^r = 1$. Proposition 1 suggests that $O_{\rm SISO} = \frac{\pi}{C(\alpha)} \frac{\sum_{i\in\mathcal{K}} \lambda_i P_i^{\check{\alpha}} \beta_i^{-\check{\alpha}}}{\sum_{j\in\mathcal{K}} \lambda_j P_j^{\check{\alpha}}}$, where $C(\alpha) = \tilde{C}(\alpha)\Gamma(1+\check{\alpha})$. Note that $O_{\rm SISO}$ is equivalent to the coverage probability derived in [16] for single antenna systems.

B. Single-Input Multiple-Output (SIMO) Systems

For the SIMO systems, we set $S_i = 1$, $\forall i$ and Proposition 1 reduces to $O_{\rm SIMO}^{\rm ZF} = O_{\rm SISO}\Omega$, where $\Omega = \sum_{r=0}^{N^r-1} \frac{\Gamma(\check{\alpha}+r)}{\Gamma(\check{\alpha})\Gamma(1+r)}$. Applying Kershaws inequality [37], thus $\sum_{r=0}^{N^r-1} \left(r-0.5+\sqrt{\check{\alpha}+0.25}\right)^{\check{\alpha}-1} \leq \Omega \leq \sum_{r=0}^{N^r-1} (r+0.5\check{\alpha})^{\check{\alpha}-1}$, or $\int_0^{N^r-1} \left(x-0.5+\sqrt{\check{\alpha}+0.25}\right)^{\check{\alpha}-1} \mathrm{d}x \lessapprox \Omega \lessapprox \int_0^{N^r-1} (x+0.5\check{\alpha})^{\check{\alpha}-1}\,\mathrm{d}x$. Therefore, $\frac{\alpha}{2}\left(N^r+\sqrt{\check{\alpha}+0.25}\right)^{\check{\alpha}-1} \lessapprox \frac{O_{\rm SIMO}^{\rm ZF}}{O_{\rm SISO}} \lessapprox \frac{\alpha}{2}(N^r+0.5\check{\alpha})^{\check{\alpha}-1}$. This last expression indicates that $\frac{O_{\rm SIMO}^{\rm ZF}}{O_{\rm SISO}} \propto (N^r)^{\check{\alpha}}$, which is an increasing function of N^r. In Fig. 1, $\frac{O_{\rm SIMO}^{\rm ZF}}{O_{\rm SISO}}$ is plotted vs. α, and N^r. Increasing the number of receive antennas is shown to make a greater performance gain for small values of α. The impact of a large path-loss exponent can also be compensated by increasing the number of receive antennas.

C. Multiple-Input Single-Output (MISO) Systems

So far, we have assumed that the CSIT is not provided. However, some cases with CSIT known at the BSs can also be covered by our analysis. Let's consider a MISO system, where $N^r = 1$, and $S_i = 1$, $\forall i$ and assume that CSIT is available to the BSs utilized for eigen beamforming, i.e., maximum ratio transmission (MRT) [7]. In such a system, the SIR at the typical UE served by x_i is

$$\mathrm{SIR}_{x_i}^{\rm MRT} = \frac{P_i \|x_i\|^{-\alpha} H_{x_i}^{\rm MRT}}{\sum_{j\in\mathcal{K}} \sum_{x_j\in\Phi_j/x_i} P_j \|x_j\|^{-\alpha} G_{x_j}^{\rm MRT}}, \tag{12}$$

where $H_{x_i}^{\rm MRT}$ and $G_{x_j}^{\rm MRT}$ are Chi-squared with $2N_i^t$ DoF, and exponential random variables, respectively. Using Proposition 1, the coverage probability is thus

$$O_{\rm MISO}^{\rm MRT} = \frac{\pi}{C(\alpha)} \frac{\sum_{i\in\mathcal{K}} \lambda_i \left(\frac{P_i}{\beta_i}\right)^{\check{\alpha}} \sum_{m=0}^{N_i^t-1} \frac{\Gamma(\check{\alpha}+m)}{\Gamma(\check{\alpha})\Gamma(1+m)}}{\sum_{j\in\mathcal{K}} \lambda_j P_j^{\check{\alpha}}}. \tag{13}$$

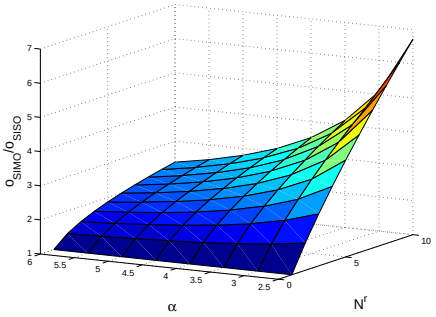

Fig. 1. $\frac{O_{\rm SIMO}^{\rm ZF}}{O_{\rm SISO}}$ *v.s.* α and N^r.

By applying Kershaw's inequality, $\frac{O^{\mathrm{MRT}}_{\mathrm{MISO}}}{O_{\mathrm{SISO}}} \leq$

$$\frac{\sum_{i\in\mathcal{K}}\lambda_i\left(\frac{P_i}{\beta_i}\right)^{\check{\alpha}}\sum_{m=0}^{N_i^t-1}\frac{\Gamma(\check{\alpha}+m)}{\Gamma(\check{\alpha})\Gamma(1+m)}}{\sum_{i\in\mathcal{K}}\lambda_i\left(\frac{P_i}{\beta_i}\right)^{\check{\alpha}}} \propto \frac{\alpha}{2\Gamma(\alpha)}\frac{\sum_{i\in\mathcal{K}}\lambda_i\left(N_i^t\frac{P_i}{\beta_i}\right)^{\check{\alpha}}}{\sum_{i\in\mathcal{K}}\lambda_i\left(\frac{P_i}{\beta_i}\right)^{\check{\alpha}}}.$$

On the other hand, $\frac{O^{\mathrm{MRT}}_{\mathrm{MISO}}}{O^{\mathrm{ZF}}_{\mathrm{SIMO}}} \propto \frac{\sum_{i\in\mathcal{K}}\lambda_i\left(\frac{N_i^t}{N^r}\frac{P_i}{\beta_i}\right)^{\check{\alpha}}}{\sum_{i\in\mathcal{K}}\lambda_i\left(\frac{P_i}{\beta_i}\right)^{\check{\alpha}}}$. In practice, $N_i^t \geq N^r$, therefore $\frac{O^{\mathrm{MRT}}_{\mathrm{MISO}}}{O^{\mathrm{ZF}}_{\mathrm{SIMO}}} \geq 1$.

D. MISO-SDMA Systems

Another example scenario in which the BSs have access to the CSIT, is the MISO-SDMA system. Let $N^r = 1$, and $S_i = 1$, $\forall i$. We further assume that each cell of tier i serves $U_i \leq N_i^t$ UEs adopting ZFBF at the transmitter (see [29], [26] for more information). Assuming a fixed transmit power, the SIR of the typical UE that is associated with BS x_i is

$$\mathrm{SIR}^{\mathrm{MRT}}_{x_i} = \frac{\frac{P_i}{U_i}\|x_i\|^{-\alpha}H^{\mathrm{SDMA}}_{x_i}}{\sum_{j\in\mathcal{K}}\sum_{x_j\in\Phi_j/x_i}\frac{P_j}{U_j}\|x_j\|^{-\alpha}G^{\mathrm{SDMA}}_{x_j}}, \tag{14}$$

where $H^{\mathrm{SDMA}}_{x_i}$ and $G^{\mathrm{SDMA}}_{x_j}$ are both Chi-squared random variables with $2(N_i^t - U_i + 1)$ and DoF of $2U_j$, respectively [26], [25]. Using Proposition 1, we then obtain

$$O^{\mathrm{SDMA}}_{\mathrm{MISO}} = \frac{\pi}{\tilde{C}(\alpha)}\frac{\sum_{i\in\mathcal{K}}\lambda_i\left(\frac{P_i}{U_i\beta_i}\right)^{\check{\alpha}}\sum_{m=0}^{N_i^t-U_i}\frac{\Gamma(\check{\alpha}+m)}{\Gamma(\check{\alpha})\Gamma(1+m)}}{\sum_{j\in\mathcal{K}}\lambda_j(\frac{P_j}{U_j})^{\check{\alpha}}\frac{\Gamma(\check{\alpha}+U_j)}{\Gamma(U_j)}}. \tag{15}$$

Remark 1: For the cases of SISO, SIMO, MISO-MRT, and MISO-SDMA, the above-obtained bounds are accurate when $\beta_i > 1$ $\forall i$. To the best of our knowledge there are no closed-form expressions of the coverage probability.

Fig. 2 shows that for $U_2 = S_2 = 1$ both ZF-FRT and SDMA perform similarly. Furthermore, by increasing S_1, equivalently U_1, the coverage probability in both systems is slightly reduced. Nevertheless, for the setting, where $U_2 = S_2 = 3$, the coverage probability is reduced in both systems while SDMA system over-performs ZF-FRT system. Multi-stream ZF-FRT system and multi-user SDMA system are fundamentally different as in the former all the transmitted streams to a user are required to be successfully received to consider that user in the coverage. Therefore, by fixing the density of the BSs the likelihood of successful reception of all streams might be generally lower. Nevertheless, in the multi-user SDMA each UE is only responsible for detecting its own single stream data. Of course the likelihood of successful reception for each individual stream might also reduce by increasing the number of UEs due to reduction of DoF and ICI increase however, the reduction is less than that of the ZF-FRT scheme. In terms of the complexity, multi-user SDMA for each UE requires perfect channel direction information to be able to construct the precoding matrix, whereas the ZF-FRT scheme does not require any feedback.

E. Orthogonal Space-Time Block Codes (OSTBCs) Systems

Recognizing the statistical resemblances of the SIR expressions among ZFBF and OSTBCs systems (see, e.g., [20]), the analysis of this paper can readily be extended to the case of OSTBC systems. To do so, we need to assume that fading matrices, the positions of BSs and UEs, and their associations remain unchanged during the the space-time block codes. Analyzing schemes, such as maximum ration combining (MRC) at the receiver while the transmitters do not have CSIT, are more complex due to the inter-stream interference at the receiver side.

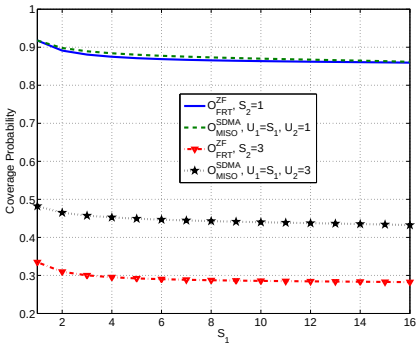

Fig. 2. Coverage probability of ZFBF and MISO-SDMA systems *vs.* S_1, where $\lambda_1 = 10^{-4}$, $\lambda_2 = 5\times10^{-3}$, $\alpha = 4$, $N^r = N_1^t = N_2^t = 16$, $P_1 = 50$W, $P_1 = 10$W, $\beta_1 = 10$dB, $\beta_2 = 5$.

VI. Numerical Analysis and Simulation Results

We now provide numerical and simulation results. $K = 2$ is assumed for easier presentation of the results. We first focus on providing numerical analysis of coverage performance of FRT and ART schemes, aiming to shed light how multiplexing gains affect the strength of intending signals and interference. We then provide technical interpretations of the observed trends.

The second part of this section provides various simulation results to corroborate our analysis and investigate the impacts of densification and MIMO communications on the coverage performance. We also investigate the cases in which densification and MIMO communications are beneficial to the network's coverage performance.

A. Numerical Analysis

To capture the impact of multiplexing gains on the coverage probability, we simply assume $\beta_i = \beta$ and $\lambda_i = \lambda$ and $P_i = P$.

1) The FRT Scheme: We start with the FRT scheme. Proposition 1 provides an upper-bound of the coverage probability. Here we consider the coverage probability for tier i in (6). Examination of (6) reveals two impacts of multiplexing gains: (*i*) the DoF of intending and interfering signals and (*ii*) the transmission power per stream on both attending and interfering signals. To distinguish them, we first exclude the impact of multiplexing gains on the transmission power per stream (it is equivalent to saying that the transmission power at BSs of tier j proportionally increases with S_j)). We then define $f_1(S_1) \triangleq \frac{1}{S_1^{\check{\alpha}}}\left(\sum_{r_1=0}^{N^r-S_1}\frac{\Gamma(\frac{\check{\alpha}}{S_1}+r_1)}{\Gamma(\frac{\check{\alpha}}{S_1})\Gamma(1+r_1)}\right)^{S_1}$ and $f_2(S_1,S_2) \triangleq \left(\frac{\Gamma(\frac{\check{\alpha}}{S_1}+S_2)}{\Gamma(S_2)}\right)^{S_1} + \left(\frac{\Gamma(\frac{\check{\alpha}}{S_1}+S_1)}{\Gamma(S_1)}\right)^{S_1}$. It is easy to observe that functions, $f_1(S_1)$ and $f_2(S_1,S_2)$ represent the

effect of multiplexing gains, S_1, and S_2, in the numerator and the denominator of (6) while the impact of power per stream is excluded. Moreover, we introduce functions $f_1^*(S_1)$ and $f_2^*(S_1,S_2)$, respectively, as $f_1^*(S_1) \triangleq S_1^{-\breve{\alpha}} f_1(S_1)$ and $f_2^*(S_1,S_2) \triangleq S_2^{-\breve{\alpha}} \left(\frac{\Gamma(\frac{\breve{\alpha}}{S_1}+S_2)}{\Gamma(S_2)}\right)^{S_1} + S_1^{-\breve{\alpha}} \left(\frac{\Gamma(\frac{\breve{\alpha}}{S_1}+S_1)}{\Gamma(S_1)}\right)^{S_1}$ so that the impacts of multiplexing gains on the transmit powers at the BSs are also captured. As it is seen from (6), $O_{\text{FRT},1}^{\text{ZF}} \propto \frac{f_1^*(S_1)}{f_2^*(S_1,S_2)}$. Functions $f_1(S_1)$ and $f_1^*(S_1)$ can be interpreted as *tangible intended-DoF per communication link*, and *effective intended-power per communication link*, respectively. Similarly, to capture the impact of multiplexing gains on the coverage performance per stream in (7), we define $g_1(S_1) \triangleq \sum_{r_1=0}^{N^r-S_1} \frac{\Gamma(\breve{\alpha}+r_1)}{\Gamma(\breve{\alpha})\Gamma(1+r_1)}$ and $g_2(S_1,S_2) \triangleq \frac{\Gamma(\breve{\alpha}+S_2)}{\Gamma(S_2)} + \frac{\Gamma(\breve{\alpha}+S_1)}{\Gamma(S_1)}$, while the effect of multiplexing gains on the power per stream is excluded. To incorporate this, we further define $g_1^*(S_1) \triangleq S_1^{-\breve{\alpha}} g_1(S_1)$ and $g_2^*(S_1,S_2) \triangleq S_2^{-\breve{\alpha}} \frac{\Gamma(\breve{\alpha}+S_2)}{\Gamma(S_2)} + S_1^{-\breve{\alpha}} \frac{\Gamma(\breve{\alpha}+S_1)}{\Gamma(S_1)}$. It is then easy to verify from (7) that $O_{\text{FRT},1,l_i}^{\text{ZF}} \propto \frac{g_1^*(S_1)}{g_2^*(S_1,S_2)}$.

On the other hand, to inspect the impact of multiplexing gains in the terms of signal detection vs. DoF behavior, we also define $h_1(S_1) \triangleq \mathbb{E}[\min_{l=1,\ldots,S_1} \chi^2_{2(N^r-S_1+1)}]$, as an approximation of the *expected intended-DoF per communication link*, where χ^2_{2m} stands for Chi-squared r.v. with DoF m and is obtained from

$$h_1(S) = S \int_0^\infty e^{-g} \frac{g^{N^r-S+1}}{\Gamma(S)} \left(\int_g^\infty e^{-y} \frac{y^{N^r-S}}{\Gamma(S)} dy \right)^{S-1} dg$$

$$= S \int_0^\infty \left(e^{-g} \sum_{l=0}^{N^r-S} \frac{g^l}{l!} \right)^{S-1} \frac{g^{N^r-S+1} e^{-g}}{(S-1)!} dg$$

$$= \frac{S(N^r-S)!}{(S-1)!} \int_0^\infty e^{-Sg} \sum_{k_1+\ldots+k_{N^r-S}=S-1} \frac{g^{N^r-S+1+\sum_{l=0}^{N^r-S} lk_l}}{\prod_{l=0}^{N^r-S} k_l!(l!)^{k_l}} dg$$

$$= \frac{S(N^r-S)!}{(S-1)!} \sum_{k_1+\ldots+k_{N^r-S}=S-1} \frac{\int_0^\infty e^{-Sg} g^{N^r-S+1+\sum_{l=0}^{N^r-S} lk_l} dg}{\prod_{l=0}^{N^r-S} k_l!(l!)^{k_l}}$$

$$= \sum_{k_1+\ldots+k_{N^r-S}=S-1} \frac{\frac{S(N^r-S)!}{(S-1)!}(N^r-S+1+\sum_{l=0}^{N^r-S} lk_l)!}{S^{N^r-S+2+\sum_{l=0}^{N^r-S} lk_l} \prod_{l=0}^{N^r-S} k_l!(l!)^{k_l}}.$$

This way, $k_1(S_1) \triangleq N^r - S_1 + 1$ is actually the *expected intended-DoF per stream*. Contrasting $h_1(S_1)$ ($k_1(S_1)$) against functions $f_1(S_1)$ and $f_2(S_1,S_2)$ ($g_1(S_1)$ and $g_2(S_1,S_2)$) reveals how much of the expected DoF is actually helpful in improving the ability of the receivers in detecting signals. Finally, we define $h_1^*(S_1) = S_1^{-\breve{\alpha}} h_1(S_1)$ and $g_1^*(S_1) = S_1^{-\breve{\alpha}} g_1(S_1)$ as the overall representations of the multiplexing gains on the expected DoF per link and per stream, respectively.

Fig. 3 plots $f_1(S_1)$ and $g_1(S_1)$ vs. S_1. Both $f_1(S_1)$ and $g_1(S_1)$ are shown to be monotonically decreasing functions of S_1, and hence increasing the multiplexing gain S_1 results in a lower coverage probability from both link and stream perspectives. Further, $f_1(S_1)$ is shown to be smaller than $g_1(S_1)$, so per-link coverage probability is much smaller than the that of per-stream. Therefore, per-link and per-stream coverage probabilities react differently to changes in the multiplexing gain.

We further study the impact of transmission power in Fig. 3, where $f_1^*(S_1)$ and $g_1^*(S_1)$ are presented for various multiplexing gains. Figs. 3 shows similar patterns. The main difference is that by increasing S_1, $f_1^*(S_1)$ and $g_1^*(S_1)$ decline more quickly than $f_1(S_1)$ and $g_1(S_1)$. Moreover, we observe that values of functions $f_1(S_1)$ and $g_1(S_1)$ are in general much smaller than that of $h_1(S_1)$ and $k_1(S_1)$, respectively. Consequently, the expected DoF can be considered as optimistic measures of the receiver's capability in terms of signal detection.

Fig. 4 demonstrates $f_2(S_1,S_2)$ and $g_2(S_1,S_2)$. Both functions are shown to exhibit the same pattern by varying S_1 and S_2, where generally $f_2(S_1,S_2) \leq g_2(S_1,S_2)$. Therefore, by reducing the multiplexing gain, S_1, the negative impact of ICI on the performance of a communication link is reduced, compared to the performance of a given stream. We also observe that by increasing S_2, both functions are increased. By incorporating the impact of power, however, the observed behavior is dramatically changed as shown in Fig. 4, where $f_2^*(S_1,S_2)$ and $g_2^*(S_1,S_2)$ are given *vs.* S_1. One can see that (*i*) there are meaningful discrepancies between functions $f_2^*(S_1,S_2)$ and $g_2^*(S_1,S_2)$ not only from their corresponding values but also from their behaviors with respect to S_1; (*ii*) while $f_2(S_1,S_2)$ and $g_2(S_1,S_2)$ are monotonically increasing functions of S_1 (left plot), $f_2^*(S_1,S_2)$ demonstrated decreasing and mildly increasing patterns depending on S_1. Function $g_2^*(S_1,S_2)$ is also slightly increased by increasing S_1.

Combining the findings of Figs. 3 and 4, we conclude that increasing the multiplexing gains reduces the coverage probability. Furthermore, the main reason for higher multiplex gains resulting in a smaller coverage probability is due to the impairing impact of multiplexing gains on the effective intended-power per communication link, noticing the flat response of function $f_2^*(S_1,S_2)$ to S_1 in Fig. 4 as well as a sharp drop of function $f_1^*(S_1)$ to S_1 in Fig. 3. To confirm this conclusion, we set $S_1 = S_2 = S$, and illustrate per-link coverage probability (6) and per-stream coverage probability (7) vs. parameter S in Fig. 5. Both interpretations of the coverage probabilities are shown to be monotonically decreasing functions of S. According to Fig. 5, increasing the multiplexing gain from $S = 1$ to $S = 2$ reduces the coverage probability per link by more than 30%, with an almost 15% reduction in the coverage probability per stream.

For $N^r = S_i$, $\forall i$,

$$O_{\text{FRT}}^{\text{ZF}} \leq \frac{\pi}{\tilde{C}(\alpha)\beta^{\breve{\alpha}}} \frac{1}{S^{\breve{\alpha}}} \left(\frac{\Gamma(S)}{\Gamma(\breve{\alpha}/S+S)} \right)^S. \tag{16}$$

Using Kershaws inequality (see, e.g., [37]), we write

$$\frac{\Gamma(\frac{\breve{\alpha}}{S}+S)}{\Gamma(S)} > \left(S + \frac{\breve{\alpha}}{S} - 1 + \frac{1-\breve{\alpha}/S}{2} \right)^{\frac{\breve{\alpha}}{S}} = \left(S + \frac{\frac{\breve{\alpha}}{S}-1}{2} \right)^{\breve{\alpha}/S}. \tag{17}$$

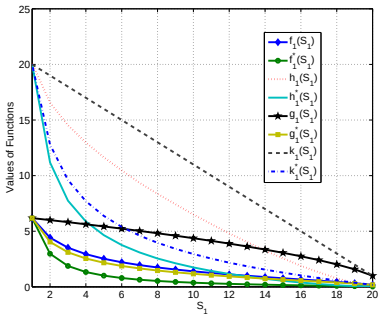

Fig. 3. $f_1(S_1)$, $g_1(S_1)$, $h_1(S_1)$, and $k_1(S_1)$ *vs.* S_1 for $K = 2$, $N^r = 20$, and $\alpha = 3.5$.

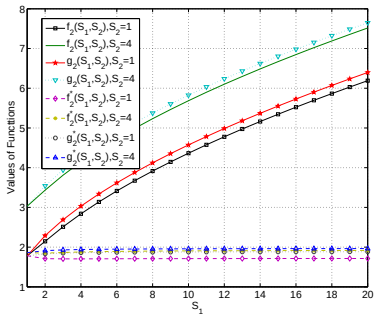

Fig. 4. $f_1^*(S_1)$, $g_1^*(S_1)$, $h_1^*(S_1)$, and $k_1^*(S_1)$ *vs.* S_1 for $K = 2$, $N^r = 20$, and $\alpha = 3.5$.

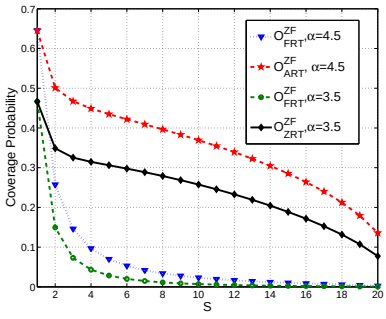

Fig. 5. Coverage probability of the ART and FRT schemes *vs.* S, where $\lambda_i = \lambda$, $P_i = P$, and $\beta_i = \beta$, $\forall i$.

Substituting (17) into (16) yields $O_{\text{FRT}}^{\text{ZF}} \leq \frac{\pi}{\tilde{C}(\alpha)\beta^{\breve{\alpha}}} \frac{1}{S^{\breve{\alpha}(1-S^{-1})}} \left(1 + \frac{\breve{\alpha}/S-1}{2S}\right)^{-\breve{\alpha}}$ which is a decreasing function of S. Thus, increasing the multiplexing gain S reduces the coverage probability.

Note that the above numerical and analytical results are based on the upper-bound given in Proposition 1. The simulation results presented in the next subsection confirm the accuracy of Proposition 1, and thus the conclusions drawn here remain valid.

2) The ART Scheme: **We consider ART scheme for which the corresponding coverage probability is approximated in Proposition 2. According to Proposition 2, its coverage probability is proportionally related to the coverage probability of FRT. Thus, the above numerical analysis would stay valid in the case of ART. Note that comparing with the bound for the coverage probability of the FRT scheme given in (5), understanding the impact of the multiplexing gains even in the simplified scenario of this subsection is not straightforward. Therefore, we rely on a numerical analysis by comparing the approximation in (11) with the bound given in Proposition 1.**

In Fig. 5, (5) and (11) are plotted for a system with $K = 2$, and $S_1 = S_2 = S$. The ART scheme is shown to perform significantly better than FRT. For instance, when $S = 4$, and $\alpha = 4.5$, adopting the ART scheme makes a more than 45% coverage performance improvement over the system with FRT. The modest cost of this improvement is the extra signaling overhead caused by the UEs feeding back to the BSs the achievable data rates for each stream. Fig. 5 also suggests that compared to the FRT scheme, in the ART scheme the coverage performance diminishes faster by increasing the multiplexing gain. For instance, by increasing the multiplexing gain from $S = 1$ to $S = 2$, the coverage performance of FRT (ART) is reduced by 30% (10%). Fig. 5 further indicates that the coverage performance of ART is more sensitive to the variation of the path-loss exponent than that of FRT. Therefore, the FRT scheme demonstrates a level of robustness against changes (e.g., from outdoor to indoor) in the wireless environment.

B. Simulation Results

In our simulation we set $K = 2$ and randomly locate BSs of each tier in a disk of radius 10000 units according to the corresponding deploying density. All BSs are always active and the simulation is run for 40000 snapshots. In each snapshot, we randomly generate MIMO channels based on the corresponding multiplexing gains at the BSs.

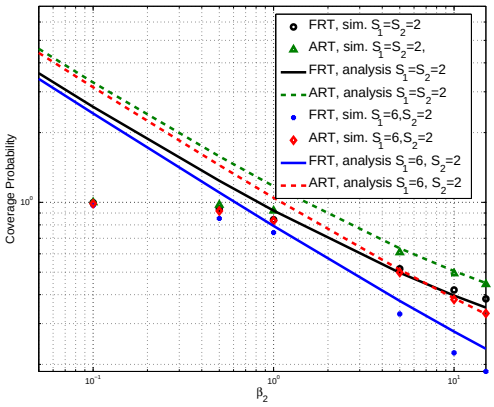

Fig. 6. Coverage probability of the FRT and ART scheme *v.s.* β_2, where $\lambda_1 = 10^{-4}$, $\lambda_2 = 5 \times 10^{-4}$, $\alpha = 4$, $N^r = 10$, $P_1 = 50$W, $P_1 = 10$W, $\beta_1 = 5$.

1) Accuracy of the Bounds: Fig. 6 plots the coverage probabilities under FRT and ART schemes *vs.* β_2. As shown for $\beta_2 \geq 1$, which is the case of our model, the analytical bounds closely follow the simulation results. This finding is important especially for the case of ART as the proposed bound in (11) is heuristic. For the case of $\beta_2 < 1$, however, the analysis is not representative. Therefore, Fig. 6 confirms the results reported in [16], [26]. We further observe that by increasing β_2, the coverage probability is reduced in all graphs and ART outperforms FRT. In both schemes, by increasing the multiplexing gain, S_1, the corresponding coverage probabilities are shown to be reduced.

Fig. 7 compares the analysis and simulation results *vs.* β_1, showing the same patterns observed in Fig. 6. However, comparison of Figs. 6 and 7 shows that increasing β_1 makes less impact on reduction of the coverage probability in both schemes.

From the comparison of Figs. 7 and 6, we also find that increasing β_2 widens the gap between FRT and ART while the growth of β_1 narrows the gap. The observed discrepancies are due to the differences between the transmission power and densities of the BSs in different tiers.

We also evaluate the accuracy of our analysis against the

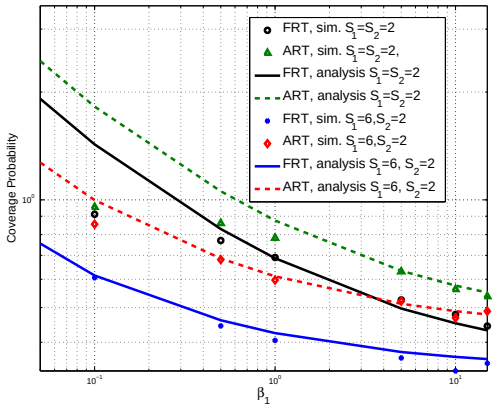

Fig. 7. Coverage probability of FRT and ART scheme *v.s.* β_1 where $\lambda_1 = 10^{-4}$, $\lambda_2 = 5 \times 10^{-4}$, $\alpha = 4$, $N^r = 10$, $P_1 = 50$W, $P_1 = 10$W, $\beta_2 = 5$.

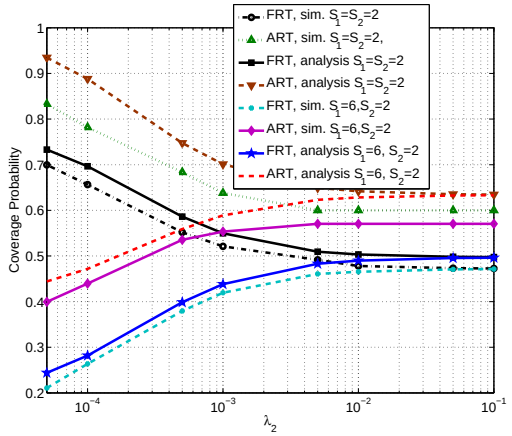

Fig. 8. Coverage probability of the FRT and ART schemes *vs.* λ_2, where $\lambda_1 = 10^{-4}$, $\alpha = 4$, $N^r = 10$, $P_1 = 50$ W, $P_1 = 10$W, $\beta_1 = 2$, and $\beta_2 = 5$.

density of BSs deployment in Figs. 8 and 9. In the former (the latter), we fix $\lambda_1 = 10^{-4}$ ($\lambda_2 = 10^{-4}$) and change λ_2 (λ_1). Both figures confirm that the proposed approximations for both FRT and ART closely follow the corresponding coverage probability. This also confirms our conclusion on the impact of the multiplexing gains on the coverage performance of FRT and ART in the previous sections.

2) Impact of Multiplexing Gains and Densifications: Figs. 8 and 9 also highlight the following important trends. (*i*) ART provides better coverage performance than FRT by almost 20–25%, which is smaller than our previously expected value in Section IV-B. This is because in Section IV-B, transmission powers, deploying densities, and SIR thresholds are assumed to be the same in both tiers. One may conclude that the advantage of ART over FRT is fully exploitable in a homogenous network deployment, i.e., $P_i = P$, $S_i = S$, $\lambda_i = \lambda$, and $\beta_i = \beta$ $\forall i$. (*ii*) Multiplexing gains S_1 and S_2 make different impacts on the coverage performance: (*ii-1*) According to Fig. 8, while the density of high-power BSs in tier 1, λ_1, is fixed, if $S_1 = S_2$, increasing λ_2 lowers the coverage probability. On the contrary, Fig. 9 indicates that when the density of low-power BSs in tier 2, λ_2, is fixed by increasing λ_1, a higher coverage performance results for $S_1 = S_2$. In fact, for cases with the same multiplexing gain across the tiers, the coverage probability could decrease/increase depending upon the densified tier. Therefore, in such cases it is more efficient to densify the tier with the higher transmission power. (*ii-2*) Fig. 8 shows that for fixed λ_1, increasing λ_2 is beneficial and results in a higher coverage performance, where $S_1 = 6$, and $S_2 = 2$. Fig. 9, on the other hand, illustrates that for $S_1 = 6$ and $S_2 = 2$ and when λ_2 is fixed, increasing λ_1 lowers the coverage probability. Consequently, in cases with different multiplexing gains, the results suggest that it is better to densify the tier with low-power and/or low multiplexing gain. (*ii-3*) For high values of λ_2, Fig. 8 also shows that both cases of $S_1 = 6$, $S_2 = 2$ and $S_1 = S_2 = 2$ perform the same. For high values of λ_1, Fig. 9, however, shows a large gap between the coverage probability of system $S_1 = 6$, $S_2 = 2$ and that of system $S_1 = S_2 = 2$. In other words, for a network with ultra-dense low-power tier, the multiplexing gain of high-power tier can be increased without compromising the coverage performance.

In summary, increasing the density of low power BSs (tier 2) should be interpreted as a green light for increasing the multiplexing gain of tier 1 without hurting the coverage performance. Moreover, densification in tier 1 results in a higher performance provided that similar multiplexing gains are set across all tiers.

(*iii*) The results in Figs. 8 and 9 also indicate that increasing the density of low power BSs of tier 2 makes greater impact on the coverage probability than it does in tier 1. For instance, a 10-fold densification of tier 2 (tier 1) changes the coverage performance by more than 25% (10%). This is a very important practical insight because *installing more low-power BSs is cheaper than increasing the density of high-power BSs of tier 1*.

(*iv*)The above results also confirm that for large values of λ_1 and λ_2, the coverage probability is stable and does not react to densification. This is also referred to as *scale invariancy*, see, [16]. This indicates that we could increase the capacity by installing more BSs without hurting the coverage. As a result, without sacrificing the coverage performance, we can increase the density of BSs in tier 2 to simultaneously increase the multiplexing gain of tier 1.

3) Impact of Number of Receive Antennas: In Figs. 10 and 11, we study the impact of the number of receive antennas N^r on the coverage performance. We first review the results of Fig. 10, where a sparse tier 1 with the density of BSs, $\lambda_1 = 5 \times 10^{-5}$, is considered. Two scenarios are considered with respective to the density of BSs in tier 2: (1) dense, the results of which are shown in the left plot, and (2) sparse, the results of which are given in the right panel. In both cases, we investigate three cases: (1) $S_1 = S_2 = 1$, (2) $S_1 = N^r$, $S_2 = 1$, and (3) $S_1 = S_2 = N^r$. In both dense and sparse scenarios, the case of $S_1 = S_2 = N^r$ performs very poorly and increasing the number of antennas worsens performance. In this case, ART slightly outperforms FRT. Moreover, for small values of N^r, the sparse scenario yields a better performance than that of the dense scenario. For large values of N^r,

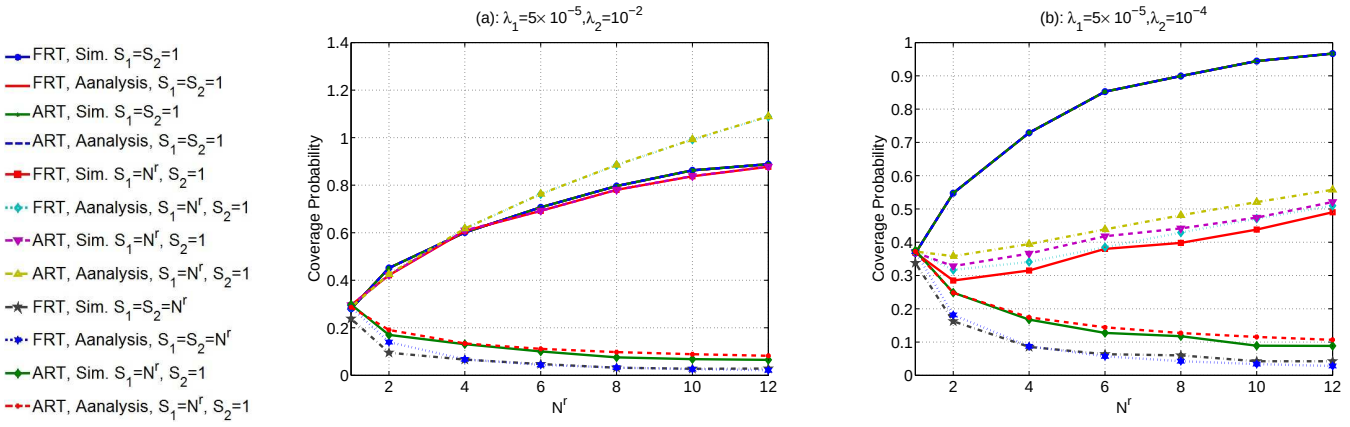

Fig. 10. Coverage probability of the FRT and ART schemes *v.s.* N^r. a: $\lambda_2 = 10^{-2}$. b: $\lambda_2 = 10^{-4}$. In both plots $\lambda_1 = 5 \times 10^{-5}$, $\alpha = 4$, $P_1 = 50$W, $P_1 = 20$W, $\beta_1 = 2$, and $\beta_2 = 5$.

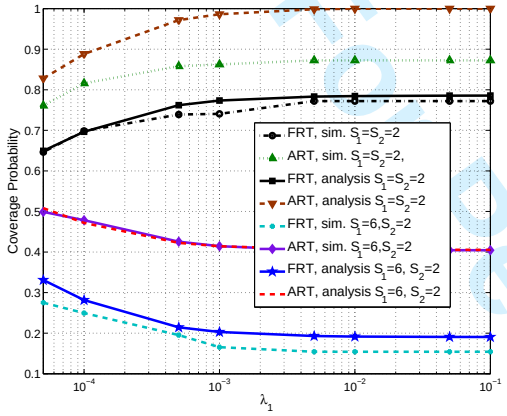

Fig. 9. Coverage probability of FRT and ART schemes *vs.* λ_1 where $\lambda_2 = 10^{-4}$, $\alpha = 4$, $N^r = 10$, $P_1 = 50$ W, $P_1 = 10$W, $\beta_1 = 2$, and $\beta_2 = 5$.

however, both scenarios perform almost the same.

Note that increasing N^r improves the coverage probability in both dense and sparse cases for $S_1 = S_2 = 1$. Besides, comparison of the left and right figures shows that the density of tier 2 has a minor impact on the coverage performance. It is also seen that the ART scheme does not make a major improvement over FRT in this case.

The case of $S_1 = N^r$, $S_2 = 1$ behaves distinctively against increasing N^r. Recall that the first tier is sparse. In the scenario that tier 2 is also sparse (Fig. 10.b) increasing N^r and thus the multiplexing gain of tier 1 has a modest impact on the coverage performance, and the ART scheme slightly improve the coverage performance compared to the FRT scheme. Nevertheless, for a dense tier 2, as the left plot indicates, the case of $S_1 = N^r$ and $S_2 = 1$ performs almost the same as the case of $S_1 = S_2 = 1$. Similarly, ART does not make any improvement over FRT. Furthermore, increasing N^r and thus S_1, $S_2 = 1$ improves the coverage probability.

Now, let's look at Fig. 11 in which we have fixed the density of tier 2 to $\lambda_2 = 5 \times 10^{-5}$ and investigate the coverage performance against N^r for both scenarios where tier 1 is sparse (the right figure) and dense (the left figure). We again consider three cases: (1) $S_1 = S_2 = 1$, (2) $S_1 = N^r$ and $S_2 = 1$, and (3) $S_1 = S_2 = N^r$. In both dense and sparse scenarios, the case of $S_1 = S_2 = N^r$ performs very poorly and increasing the number of antennas worsens performance. In this case, ART outperforms FRT. Note that comparison of both figures shows that the density of tier 1 does not have any specific impact on the coverage.

As shown in Fig. 10, the case of $S_1 = S_2 = 1$ reacts positively to the increase of N^r. In this case, both FRT and ART perform similarly.

Finally, we consider the case of $S_1 = N^r$ and $S_2 = 1$. Both figures show that the coverage performance is better than the case of $S_1 = S_2 = N^r$ but much smaller than the case of $S_1 = S_2 = 1$. Further, increasing N^r reduces the coverage probability where the the resulting reduction in the case of sparse scenario, right plot, is not as bad as the case of dense scenario, left plot. Comparing these findings with its counterpart in Fig. 10, we observe that this case is in fact reacted positively to the growth of N^r, especially in the dense scenario. Thus, if we are to apply densification in conjunction with high multiplexing gains, we suggest to keep the density of the high-power tier low and the density of low-power tier high. This allows us to increase the multiplexing gain of the high-power tier up to the number of the UE's antennas, provided that the multiplexing gain of low-power tier is kept as small as possible.

4) Impact of Path-Loss Model: **The analytical results of this paper is based on the generic path-loss model, $L_1 = \|x\|^{-\alpha}$. Here, to investigate the impact of path-loss model, we compare the coverage probability in a system with path-loss model L_1 and two other alternative path-loss models in the literature *viz.* $L_2 = \max\{1, \|x\|\}^{-\alpha}$, and $L_3 = (1 + \|x\|)^{-\alpha}$. The coverage performance of FRT, and ART schemes are presented in Fig. 12.a, and Fig. 12.b, respectively. As it is seen, regardless of multiplexing gains, for both FRT and ART schemes the systems with L_1 and L_2 path-loss models follow similar trends and achieve almost the same coverage probability. For very dense system configurations however, the coverage probability in a system with L_2 path-loss model is slightly declined. It is also seen that densification in a system with L_3 path-**

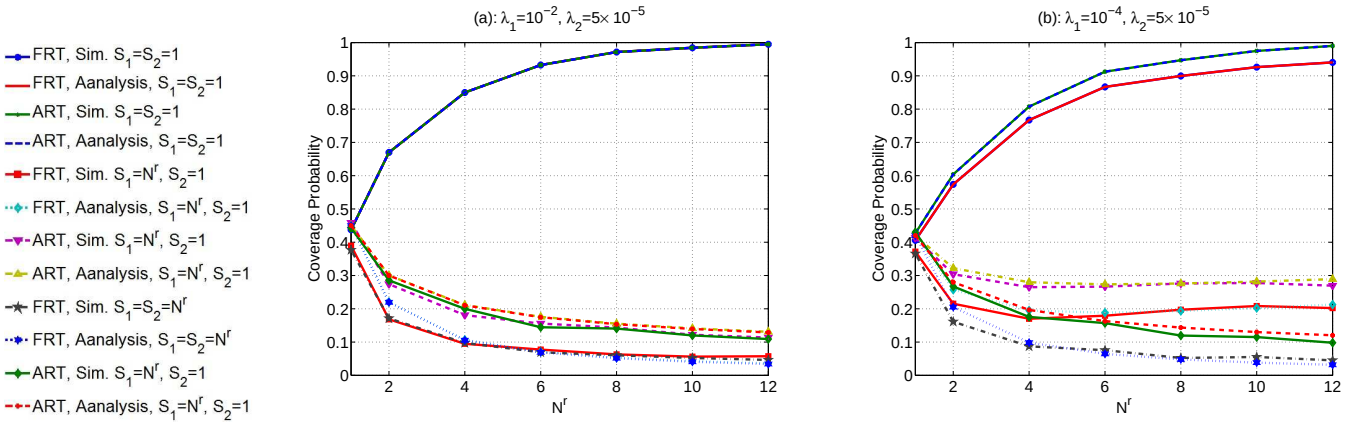

Fig. 11. Coverage probability of the FRT and ART schemes *v.s.* N^r. a: $\lambda_1 = 10^{-2}$. b: $\lambda_1 = 10^{-4}$. In both plots $\lambda_2 = 5 \times 10^{-5}$, $\alpha = 4$, $P_1 = 50$W, $P_1 = 20$W, $\beta_1 = 2$, and $\beta_2 = 5$.

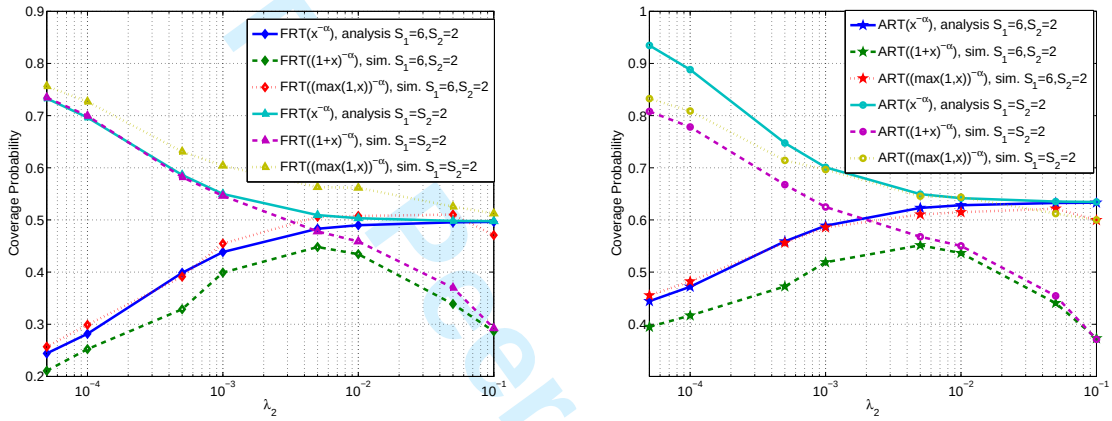

Fig. 12. a: Coverage probability of the FRT scheme *v.s.* $\lambda_2 = 10^{-4}$. b: Coverage probability of the ART scheme *v.s.* $\lambda_2 = 10^{-4}$. In both plots Coverage probability of the FRT and ART schemes *vs.* λ_2, where $\lambda_1 = 10^{-4}$, $\alpha = 4$, $N^r = 10$, $P_1 = 50$ W, $P_1 = 10$W, $\beta_1 = 2$, and $\beta_2 = 5$.

loss model results in increasing the coverage probability until a certain point after which the coverage probability is reduces (A similar result is also spotted for double-slop path-loss model in [39] for SISO systems). Finally, it is important to note that in dense deployment and for ($S_1 = S_2 = 2$) , and ($S_1 = 6$ and $S_2 = 2$), the coverage performance of FRT and ART schemes is very close regardless the path-loss model.

VII. Conclusions

In this paper, we have evaluated the coverage performance of multi-antenna (MIMO) zero-forcing beamforming (ZFBF) communications in heterogenous networks (HetNets). Our main goal was to understand the coverage performance per each communication link in multi-stream communications. By employing stochastic geometry, we studied the network-wise coverage performance. The analysis has covered both cases of fixed-rate transmission (FRT) and adaptive-rate transmission (ART). We have derived a set of closed-form approximations for the coverage performance for both FRT and ART, accuracies of which were also examined and confirmed against simulations. Our proposed bounds captured the impact of various system parameters on the coverage probability.

The main findings of our analysis and simulations were: (*i*) the larger the multiplexing gains, the lower the coverage probability; (*ii*) densification of the network is better to be practiced in low-power tiers as it paves the way for increasing the multiplexing gains of the high-power, low-density macro BSs without compromising the coverage performance; (*iii*) when dealing with multi-stream MIMO communications, the tangible DoFs in detecting the intended signals are much smaller than those of the wireless medium; (*iv*) the sensitivity of the tangible DoFs of the intended signals against the multiplexing gains was the main culprit of reducing the coverage probability with multiplexing gains; and (*iv*) increasing the multiplexing gain in a cell while all other multiplexing gains are kept intact may result in unexpected amplification of ICI.

Appendix A: Proof of Proposition 1

The following lemmas are used in proving Proposition 1.

Lemma 1: For a r.v., H, distributed according to χ^2_{2M} with CCDF $\bar{\mathrm{F}}_H(z) = e^{-z} \sum_{m=0}^{M-1} \frac{z^m}{m!}$, the inverse Laplace transform of $\bar{\mathrm{F}}_H(z)$ is $\bar{\mathcal{L}}_{\bar{\mathrm{F}}_H(z)}(t) = \sum_{m=0}^{M-1} \frac{1}{m!} \delta^{(m)}(t-1)$, where $\delta^{(m)}(t)$ is the

m-th derivative of Dirac's Delta function. Furthermore, there holds $\int_0^\infty \frac{\bar{\mathcal{L}}_{\bar{\mathrm{F}}_{H}(z)}(t)}{t^{\breve{\alpha}}}\mathrm{d}t = \sum_{m=0}^{M-1} \frac{\Gamma(\breve{\alpha}+m)}{\Gamma(\breve{\alpha})\Gamma(m+1)}$.

Proof: The proof follows the same line of argument as in the proof of Corollary 1 in [40].The only difference is that in [40] the fading distribution is Nakagami-m fading with power 1 and the CCDF is $\bar{\mathrm{F}}_H(z) = e^{-Mz}\sum_{m=0}^{M-1}\frac{M^m z^m}{m!}$. □

Lemma 2: Consider a shot noise process, $I = \sum_{j\in\mathcal{K}} I_j$, where $I_j = \sum_{x_j\in\Phi_j} P_j\|x_j\|^{-\alpha}H_{x_j}$, and H_{x_j}s are i.i.d. random variables distributed according to $\chi^2_{2M_j}$. Assume H is distributed according to χ^2_{2M} and is independent of H_{x_j}s. Then, for a given real parameter $\Delta \geq 0$

$$\mathbb{P}\{H \geq \Delta I\} = \int_0^\infty \bar{\mathcal{L}}_{\bar{\mathrm{F}}_H}(t) e^{-t^{\breve{\alpha}}\Delta^{\breve{\alpha}}\tilde{C}(\alpha)\sum_{j\in\mathcal{K}}\lambda_j P_j^{\breve{\alpha}}\frac{\Gamma(\breve{\alpha}+M_j)}{\Gamma(M_j)}}\mathrm{d}t,$$

where $\tilde{C}(\alpha) = \pi\Gamma(1-\breve{\alpha})$ and $\bar{\mathcal{L}}_{\bar{\mathrm{F}}_{H_i^{\mathrm{ZF}}}}(t_i)$ is the inverse Laplace transform of CCDF of r.v. H as given in Lemma 1.

Proof: Due to independency of processes Φ_is we get $\mathbb{P}\{H \geq \Delta I\} =$

$$\mathbb{E}\int_0^\infty \bar{\mathcal{L}}_{\bar{\mathrm{F}}_H}(t) e^{-t\Delta\sum_{j\in\mathcal{K}} I_j}\mathrm{d}t = \int_0^\infty \bar{\mathcal{L}}_{\bar{\mathrm{F}}_H}(t)\prod_{j\in\mathcal{K}}\mathcal{L}_{I_j}(t\Delta)\,\mathrm{d}t, \quad (18)$$

where $\mathcal{L}_{I_j}(t)$ is the Laplace transform of r.v. I_j and $\mathcal{L}_{I_j}(t\Delta) =$

$$\mathbb{E}e^{-t\Delta\sum_{x_j\in\Phi_j}P_j\|x_j\|^{-\alpha}H_{x_j}} = \mathbb{E}_{\Phi_j}\prod_{x_j\in\Phi_j}\mathbb{E}_{H_{x_j}}e^{-t\Delta P_j\|x_j\|^{-\alpha}H_{x_j}}$$

$$= e^{-2\pi\lambda_j\int_0^\infty[1-(1+t\Delta P_j x_j^{-\alpha})^{-M_j}]x_j dx_j} = e^{-\pi\lambda_j(t\Delta P_j)^{\breve{\alpha}}\Psi(M_j,\alpha)}, \quad (19)$$

where $\Psi(M_j,\alpha) = \int_0^\infty[1-(1+w_j^{-\alpha/2})^{-M_j}]\mathrm{d}w_j$. Applying (8) in [41] for the Laplace transform of the shot noise process, I_j, we obtain$\mathcal{L}_{I_j}(t\Delta) =$

$$e^{-\tilde{C}(\alpha)\lambda_j(t\Delta P_j)^{\breve{\alpha}}\mathbb{E}[(H_j)^{\breve{\alpha}}]} = e^{-\tilde{C}(\alpha)\lambda_j(t\Delta P_j)^{\breve{\alpha}}\frac{\Gamma(\breve{\alpha}+M_j)}{\Gamma(M_j)}}, \quad (20)$$

noticing that for Chi-squared r.v.s with M_j DoF $\mathbb{E}[(H_j)^{\breve{\alpha}}] = \frac{\Gamma(\breve{\alpha}+M_j)}{\Gamma(M_j)}$. Substituting (20) into (18) completes the proof. Note that by comparing (20) and (19), it can be shown that $\Psi(M_j,\alpha) = \frac{\tilde{C}(\alpha)}{\pi}\frac{\Gamma(\breve{\alpha}+M_j)}{\Gamma(M_j)}$. □

Proof of Proposition 1: The coverage probability is defined as the probability of the outcome in (3). According to Lemma 1 in [16], and assuming $\beta_i \geq 1$, $\forall i$ we have

$$O_{\mathrm{FRT}}^{\mathrm{ZF}} = \mathbb{P}\left\{\max_{\bigcup_{i\in\mathcal{K}} x_i\in\Phi_i}\min_{l=1,\ldots,S_i}\mathrm{SIR}_{x_i,l}^{\mathrm{ZF}} \geq \beta_i\right\}$$

$$= \sum_{i\in\mathcal{K}}\mathbb{E}\sum_{x_i\in\Phi_i} 1\left(\min_{l=1,\ldots,S_i}\mathrm{SIR}_{x_i,l}^{\mathrm{ZF}} \geq \beta_i\right). \quad (21)$$

(21) is further simplified as:

$$(21) \overset{(a)}{=} \sum_{i\in\mathcal{K}} 2\pi\lambda_i\int_0^\infty r_i\mathbb{P}\left\{\min_{l_i=1,\ldots,S_i}\mathrm{SIR}_{x_i,l_i}^{\mathrm{ZF}} \geq \beta_i\right\}\mathrm{d}r_i$$

$$\overset{(b)}{=} \sum_{i\in\mathcal{K}} 2\pi\lambda_i\int_0^\infty r_i\mathbb{E}_{\{\Phi_j\}}\prod_{l_i=1}^{S_i}\mathbb{P}\left\{\mathrm{SIR}_{x_i,l_i}^{\mathrm{ZF}} \geq \beta_i\middle|\{\Phi_j\}\right\}\mathrm{d}r_i, \quad (22)$$

where $r_i = \|x_i\|$, and (a) is due to Slivnyak- and Campbell-Mecke's Theorems [8], and in (b) we use the fact that conditioned on processes Φ_js, the SIR expressions in (2) across streams are in statistically independent. For a given r_i,$\mathbb{P}\left\{\mathrm{SIR}_{r_i,l_i}^{\mathrm{ZF}} \geq \beta_i\middle|\{\Phi_j\}\right\} =$

$$\mathbb{P}\left\{H_{r_i,l_i}^{\mathrm{ZF}} \geq \beta_i\frac{S_i}{P_i}r_i^\alpha\sum_{j\in\mathcal{K}}\sum_{x_j\in\Phi_j/x_i}\frac{P_j}{S_j}\|x_j\|^{-\alpha}G_{x_j,l_i}^{\mathrm{ZF}}\middle|\{\Phi_j\}\right\},$$

$$= \int_0^\infty \bar{\mathcal{L}}_{\bar{\mathrm{F}}_{H_i^{\mathrm{ZF}}}}(t_i)\prod_{j\in\mathcal{K}}\prod_{x_j\in\Phi_j/x_i}\mathbb{E}_{G_{x_j,l_i}^{\mathrm{ZF}}}e^{-t_i\beta_i\frac{S_i}{P_i}r_i^\alpha\frac{P_j}{S_j}\|x_j\|^{-\alpha}G_{x_j,l_i}^{\mathrm{ZF}}}\mathrm{d}t_i, \quad (23)$$

where we use (18) in Lemma 2. Since $H_{x_i,l_i}^{\mathrm{ZF}}$ are identical r.v.s, we dismiss index l_i from $\bar{\mathcal{L}}_{\bar{\mathrm{F}}_{H_i^{\mathrm{ZF}}}}(t_i)$. Substituting (23) into (22) followed by some straightforward manipulations, we get

$$(22) = \sum_{i\in\mathcal{K}} 2\pi\lambda_i\int_0^\infty r_i\mathbb{E}_{\{\Phi_j\}}\prod_{l_i=1}^{S_i}\int_0^\infty \bar{\mathcal{L}}_{\bar{\mathrm{F}}_{H_i^{\mathrm{ZF}}}}(t_i)\prod_{j\in\mathcal{K}}\prod_{x_j\in\Phi_j/x_i}$$

$$\mathbb{E}_{G_{x_j,l_i}^{\mathrm{ZF}}}e^{-t_i\beta_i\frac{S_i}{P_i}r_i^\alpha\frac{P_j}{S_j}\|x_j\|^{-\alpha}G_{x_j,l_i}^{\mathrm{ZF}}}\mathrm{d}t_i\mathrm{d}r_i$$

$$= \sum_{i\in\mathcal{K}} 2\pi\lambda_i\int_0^\infty r_i\mathrm{d}r_i\mathbb{E}_{\{\Phi_j\}}\int_0^\infty\cdots\int_0^\infty\prod_{j\in\mathcal{K}}\prod_{x_j\in\Phi_j/x_i}\prod_{l_i=1}^{S_i}$$

$$\mathbb{E}_{G_{x_j,l_i}^{\mathrm{ZF}}}e^{-\beta_i\frac{S_i}{P_i}r_i^\alpha\frac{P_j}{S_j}\|x_j\|^{-\alpha}G_{x_j,l_i}^{\mathrm{ZF}}t_{l_i}}\prod_{l_i=1}^{S_i}\bar{\mathcal{L}}_{\bar{\mathrm{F}}_{H_i^{\mathrm{ZF}}}}(t_{l_i})\mathrm{d}t_{l_i}$$

$$= \sum_{i\in\mathcal{K}} 2\pi\lambda_i\int_0^\infty r_i\mathrm{d}r_i\mathbb{E}_{\{\Phi_j\}}\int_0^\infty\cdots\int_0^\infty\prod_{j\in\mathcal{K}}\prod_{x_j\in\Phi_j/x_i}\mathbb{E}_{G_{x_j}^{\mathrm{ZF}}}$$

$$\prod_{l_i=1}^{S_i}e^{-\beta_i\frac{S_i}{P_i}r_i^\alpha\frac{P_j}{S_j}\|x_j\|^{-\alpha}G_{x_j,l_i}^{\mathrm{ZF}}t_{l_i}}\prod_{l_i=1}^{S_i}\bar{\mathcal{L}}_{\bar{\mathrm{F}}_{H_i^{\mathrm{ZF}}}}(t_{l_i})\mathrm{d}t_{l_i},$$

as $G_{x_j,l_i}^{\mathrm{ZF}}$ are i.i.d. across streams. Consequently,

$$O_{\mathrm{FRT}}^{\mathrm{ZF}} \leq \sum_{i\in\mathcal{K}} 2\pi\lambda_i\int_0^\infty r_i\mathrm{d}r_i\mathbb{E}_{\{\Phi_j\}}\int_0^\infty\cdots\int_0^\infty\prod_{j\in\mathcal{K}}\prod_{x_j\in\Phi_j/x_i}$$

$$\mathbb{E}_{G_{x_j}^{\mathrm{ZF}}}e^{-\beta_i\frac{S_i}{P_i}r_i^\alpha\frac{P_j}{S_j}\|x_j\|^{-\alpha}\sum_{l_i=1}^{S_i}G_{x_j,l_i}^{\mathrm{ZF}}t_{l_i}}\prod_{l_i=1}^{S_i}\bar{\mathcal{L}}_{\bar{\mathrm{F}}_{H_i^{\mathrm{ZF}}}}(t_{l_i})\mathrm{d}t_{l_i}$$

$$= \sum_{i\in\mathcal{K}} 2\pi\lambda_i\int_0^\infty r_i\mathrm{d}r_i\int_0^\infty\cdots\int_0^\infty\prod_{j\in\mathcal{K}}\mathbb{E}_{\Phi_j}\prod_{x_j\in\Phi_j/x_i}\mathbb{E}_{G_{x_j}^{\mathrm{ZF}}}$$

$$e^{-\beta_i\frac{S_i}{P_i}r_i^\alpha\frac{P_j}{S_j}\|x_j\|^{-\alpha}\sum_{l_i=1}^{S_i}G_{x_j,l_i}^{\mathrm{ZF}}t_{l_i}}\prod_{l_i=1}^{S_i}\bar{\mathcal{L}}_{\bar{\mathrm{F}}_{H_i^{\mathrm{ZF}}}}(t_{l_i})\mathrm{d}t_{l_i}$$

$$\overset{(a)}{=} \sum_{i\in\mathcal{K}} 2\pi\lambda_i\int_0^\infty r_i\mathrm{d}r_i\int_0^\infty\cdots\int_0^\infty\prod_{l_i=1}^{S_i}\bar{\mathcal{L}}_{\bar{\mathrm{F}}_{H_i^{\mathrm{ZF}}}}(t_{l_i})\mathrm{d}t_{l_i}$$

$$e^{-r_i^2\tilde{C}(\alpha)\left(\frac{S_i\beta_i}{P_i}\right)^{\breve{\alpha}}\sum_{j=1}^{K}\lambda_j\left(\frac{P_j}{S_j}\right)^{\breve{\alpha}}\mathbb{E}_{G_j^{\mathrm{ZF}}}\left[(\sum_{l_i=1}^{S_i}G_{j,l_i}^{\mathrm{ZF}}t_{l_i})^{\breve{\alpha}}\right]}$$

$$= \sum_{i\in\mathcal{K}} 2\pi\lambda_i\int_0^\infty\cdots\int_0^\infty\prod_{l_i=1}^{S_i}\bar{\mathcal{L}}_{\bar{\mathrm{F}}_{H_i^{\mathrm{ZF}}}}(t_{l_i})\mathrm{d}t_{l_i}$$

$$\int_0^\infty r_i e^{-r_i^2\tilde{C}(\alpha)\left(\frac{S_i\beta_i}{P_i}\right)^{\check{\alpha}}\sum_{j=1}^{K}\lambda_j\left(\frac{P_j}{S_j}\right)^{\check{\alpha}}\mathbb{E}_{G_j^{\mathrm{ZF}}}\left[(\sum_{l_i=1}^{S_i}G_{j,l_i}^{\mathrm{ZF}}t_{l_i})^{\check{\alpha}}\right]}\mathrm{d}r_i$$

$$=\sum_{i\in\mathcal{K}}\frac{\frac{\pi}{\tilde{C}(\alpha)}\lambda_i\left(\frac{P_i}{S_i\beta_i}\right)^{\check{\alpha}}\int_0^\infty\cdots\int_0^\infty\prod_{l_i=1}^{S_i}\bar{\mathcal{L}}_{\bar{\mathrm{F}}_{H_i^{\mathrm{ZF}}}}(t_{l_i})\mathrm{d}t_{l_i}}{\sum_{j\in\mathcal{K}}\lambda_j\left(\frac{P_j}{S_j}\right)^{\check{\alpha}}\mathbb{E}_{G_j^{\mathrm{ZF}}}\left[(\sum_{l_i=1}^{S_i}G_{j,l_i}^{\mathrm{ZF}}t_{l_i})^{\check{\alpha}}\right]},\qquad(24)$$

where in (a) we apply (20) in Lemma 2. Direct evaluation of (24) is complex, and hence we use the arithmetic-geometric inequality for deriving an upper-bound. Thus,

$$O_{\mathrm{FRT}}^{\mathrm{ZF}}\leq\sum_{i\in\mathcal{K}}\frac{\pi}{\tilde{C}(\alpha)}\lambda_i\left(\frac{P_i}{S_i\beta_i}\right)^{\check{\alpha}}\int_0^\infty\cdots\int_0^\infty\prod_{l_i=1}^{S_i}\bar{\mathcal{L}}_{\bar{\mathrm{F}}_{H_i^{\mathrm{ZF}}}}(t_{l_i})\mathrm{d}t_{l_i}$$

$$\frac{1}{\sum_{j\in\mathcal{K}}\lambda_j\left(\frac{P_j}{S_j}\right)^{\check{\alpha}}\mathbb{E}_{G_j^{\mathrm{ZF}}}\left[S_i^{\check{\alpha}}\left(\prod_{l_i=1}^{S_i}G_{j,l_i}^{\mathrm{ZF}}t_{l_i}\right)^{\frac{\check{\alpha}}{S_i}}\right]}$$

$$=\sum_{i\in\mathcal{K}}\frac{\frac{\pi}{\tilde{C}(\alpha)}\left(\frac{P_i}{S_i\beta_i}\right)^{\check{\alpha}}\frac{\lambda_i}{S_i^{\check{\alpha}}}\int_0^\infty\cdots\int_0^\infty\prod_{l_i=1}^{S_i}\frac{\bar{\mathcal{L}}_{\bar{\mathrm{F}}_{H_i^{\mathrm{ZF}}}}(t_{l_i})\mathrm{d}t_{l_i}}{t_{l_i}^{\frac{\check{\alpha}}{S_i}}}}{\sum_{j=1}^{K}\lambda_j\left(\frac{P_j}{S_j}\right)^{\check{\alpha}}\mathbb{E}_{G_j^{\mathrm{ZF}}}\prod_{l_i=1}^{S_i}(G_{j,l_i}^{\mathrm{ZF}})^{\frac{\check{\alpha}}{S_i}}}$$

$$=\sum_{i\in\mathcal{K}}\frac{\frac{\pi}{\tilde{C}(\alpha)}\left(\frac{P_i}{S_i\beta_i}\right)^{\check{\alpha}}\frac{\lambda_i}{S_i^{\check{\alpha}}}}{\sum_{j=1}^{K}\lambda_j\left(\frac{P_j}{S_j}\right)^{\check{\alpha}}\left(\mathbb{E}_{G_j^{\mathrm{ZF}}}(G_j^{\mathrm{ZF}})^{\frac{\check{\alpha}}{S_i}}\right)^{S_i}}\left(\int_0^\infty\frac{\bar{\mathcal{L}}_{\bar{\mathrm{F}}_{H_i^{\mathrm{ZF}}}}(t_i)}{t_i^{\frac{\check{\alpha}}{S_i}}}\mathrm{d}t_i\right)^{S_i}.\qquad(25)$$

where the last step is due to the fact that random variables $G_{x_j,l_i}^{\mathrm{ZF}}$ are i.i.d. across streams. Since H_i^{ZF} is a Chi-squared r.v. with $2(N^r-S_i+1)$ DoF using the results of Lemma 1 and Lemma 2 in (25) completes the proof. □

Appendix B: Markov's Bound

According to Markov's bound, we have

$$O_{\mathrm{ART}}^{\mathrm{ZF}}\leq\sum_{i\in\mathcal{K}}2\pi\frac{\lambda_i}{S_i\log(1+\beta_i)}\int_0^\infty r_i\sum_{l_i=1}^{S_i}\mathbb{E}\log\left(1+\mathrm{SIR}_{x_i,l_i}^{\mathrm{ZF}}\right)\mathrm{d}r_i$$

$$\overset{(a)}{=}\sum_{i\in\mathcal{K}}2\pi\frac{\lambda_i}{\log(1+\beta_i)}\int_0^\infty r_i\mathbb{E}\int_0^\infty\frac{e^{-z_i}}{z_i}\left(1-e^{-z_i\mathrm{SIR}_{x_i}^{\mathrm{ZF}}}\right)\mathrm{d}z_i\mathrm{d}r_i$$

$$\overset{(b)}{=}\sum_{i\in\mathcal{K}}2\pi\frac{\lambda_i}{\log(1+\beta_i)}\int_0^\infty r_i\int_0^\infty\frac{1}{z_i}\mathbb{E}e^{-z_i\sum_{j\in\mathcal{K}}\sum_{x_j\in\Phi_j/x_i}\frac{P_j}{S_j}x_j^{-\alpha}G_{x_j}^{\mathrm{ZF}}}$$

$$\left(1-\mathbb{E}e^{-z_i\frac{P_i}{S_i}r_i^{-\alpha}H_{x_i}^{\mathrm{ZF}}}\right)\mathrm{d}z_i\mathrm{d}r_i$$

$$\overset{(c)}{=}\sum_{i\in\mathcal{K}}2\pi\frac{\lambda_i}{\log(1+\beta_i)}\int_0^\infty r_i\int_0^\infty\frac{1}{z_i}\prod_{j\in\mathcal{K}}\mathbb{E}\mathcal{L}_{I_j}(z_i)$$

$$\left(1-\left(1+z_i\frac{P_i}{S_i}r_i^{-\alpha}\right)^{-(N_r-S_i+1)}\right)\mathrm{d}z_i\mathrm{d}r_i$$

$$\overset{(d)}{=}\sum_{i\in\mathcal{K}}2\pi\frac{\lambda_i}{\log(1+\beta_i)}\int_0^\infty\frac{1}{z_i}e^{-z_i^{\check{\alpha}}\tilde{C}(\alpha)\sum_{j\in\mathcal{K}}\lambda_jP_j^{\check{\alpha}}\frac{\Gamma(\check{\alpha}+S_j)}{S_j^{\check{\alpha}}\Gamma(S_j)}}$$

$$\int_0^\infty r_i\left(1-\left(1+z_i\frac{P_i}{S_i}r_i^{-\alpha}\right)^{-(N_r-S_i+1)}\right)\mathrm{d}r_i\mathrm{d}z_i\qquad(26)$$

where in step (a) we notice that the SIR expressions are identical among the streams and apply formula $\log(1+a)=\int_0^\infty\frac{e^{-w}}{w}(1-e^{-aw})\mathrm{d}w$ [42]; in step (b) we apply a simple change of variable; step (c) is due to independency of point processes and the fact that r.v. $H_{x_i}^{\mathrm{ZF}}$ is Chi-squared with $2(N^r-S_i+1)$ DoF; finally, in step (d) we substitute $\mathcal{L}_{I_j}(t_i)$ from Lemma 2 in Appendix A. By introducing variable $w_i=(z_iP_i/S_i)^{-\check{\alpha}}x_i^2$, (26) is further reduced to

$$(26)=\sum_{i\in\mathcal{K}}\pi\frac{\lambda_i}{\log(1+\beta_i)}\left(\frac{P_i}{S_i}\right)^{\check{\alpha}}\int_0^\infty\left(1-\frac{1}{\left(1+w_i^{-\frac{\alpha}{2}}\right)^{N_i^t-S_i+1}}\right)dw_i$$

$$\int_0^\infty z_i^{\check{\alpha}-1}e^{-z_i^{\check{\alpha}}\tilde{C}(\alpha)\sum_{j\in\mathcal{K}}\lambda_jP_j^{\check{\alpha}}\frac{\Gamma(\check{\alpha}+S_j)}{S_j^{\check{\alpha}}\Gamma(S_j)}}dz_i.$$

Using the same notation as in the proof of Lemma 2, we can write

$$\Psi(N_i^t-S_i+1,\alpha)=\int_0^\infty\left(1-\frac{1}{\left(1+w_i^{-\frac{\alpha}{2}}\right)^{N_i^t-S_i+1}}\right)dw_i$$

$$=\frac{\tilde{C}(\alpha)}{\pi}\frac{\Gamma(\check{\alpha}+N_i^t-S_i+1)}{\Gamma(N_i^t-S_i+1)}.$$

Using this, (26) is then reduced to

$$O_{\mathrm{ART}}^{\mathrm{ZF}}\leq\frac{\alpha}{2}\sum_{i\in\mathcal{K}}\frac{\frac{\lambda_i}{\log(1+\beta_i)}\left(\frac{P_i}{S_i}\right)^{\check{\alpha}}\frac{\Gamma(\check{\alpha}+N_i^t-S_i+1)}{\Gamma(N_i^t-S_i+1)}}{\sum_{j\in\mathcal{K}}\lambda_j\left(\frac{P_j}{S_j}\right)^{\check{\alpha}}\frac{\Gamma(\check{\alpha}+S_j)}{\Gamma(S_j)}}.\square\qquad(27)$$

Appendix C: Proof of Proposition 2

We write[9] $O_{\mathrm{ART}}^{\mathrm{ZF}}\approx$

$$0.5\mathbb{P}\left\{\max_{\bigcup_{i=1}^{K}x_i\in\Phi_i}S_i\min_{l_i=1,\ldots,S_i}\log\left(1+\mathrm{SIR}_{x_i,l_i}\right)\geq S_i\log(1+\beta_i)\right\}$$

$$+0.5\mathbb{P}\left\{\max_{\bigcup_{i=1}^{K}x_i\in\Phi_i}S_i\max_{l_i=1,\ldots,S_i}\log\left(1+\mathrm{SIR}_{x_i,l_i}\right)\geq S_i\log(1+\beta_i)\right\},\qquad(28)$$

where the first term is previously obtained in Proposition 1 and is equal to $O_{\mathrm{FRT}}^{\mathrm{ZF}}$. We then derive a bound of the second term as:

$$\leq\sum_{i\in\mathcal{K}}2\pi\lambda_i\int_0^\infty x_i\left(1-\mathbb{P}\left\{\max_{l=1_i,\ldots,S_i}\mathrm{SIR}_{x_i,l_i}^{\mathrm{ZF}}<\beta_i\right\}\right)\mathrm{d}x_i$$

$$=\sum_{i\in\mathcal{K}}2\pi\lambda_i\int_0^\infty r_i\mathbb{E}_{\{\Phi_j\}}(1-\prod_{l_i=1}^{S_i}(1-\mathbb{P}\{\mathrm{SIR}_{x_i}^{\mathrm{ZF}}\geq\beta_i|\{\Phi_j\}\}))\mathrm{d}r_i,\qquad(29)$$

[9] **Let us consider m identical but dependent random variables $Z_1,Z_2,\ldots Z_M$. To evaluate $\mathbb{P}\{\sum_m Z_m>R\}$ we first notice that $M\min_m Z_m\leq\sum_m Z_m\leq M\max_m Z_m$. Therefore, $\mathbb{P}\{\min Z_m>R/M\}\leq\mathbb{P}\{\sum_m Z_m>R\}\leq\mathbb{P}\{\max Z_m>R/M\}$. Using this we then approximate $\mathbb{P}\{\sum_m Z_m>R\}$ through the mean of the upper-bound and lower bound.**

in which we use the monotonicity of log function, and noting that conditioned to the PPP sets, $\{\Phi_j\}$, the SIR values are statistically independent random variables across the streams. We also represent the multiplication of probabilities associated with the streams through a summation. Since SIRs are identical random variables among the streams, we have

$$(29) = \sum_{i\in\mathcal{K}} 2\pi\lambda_i \sum_{l_i=1}^{S_i} \binom{S_i}{l_i} (-1)^{l_i+1} \int_0^\infty r_i \mathbb{E}_{\{\Phi_j\}}$$

$$\prod_{l_i'=1}^{l_i} \mathbb{P}\left\{ \mathrm{SIR}_{x_i,l_i'}^{\mathrm{ZF}} \geq \beta_i \middle| \{\Phi_j\} \right\} \mathrm{d}r_i. \tag{30}$$

Applying the same line of argument as in the proof of Proposition 1, (30) is reduced further to

$$(30) = \sum_{i\in\mathcal{K}} \frac{\pi\lambda_i}{\tilde{C}(\alpha)} \left(\frac{P_i}{S_i\beta_i}\right)^{\check{\alpha}} \sum_{l_i=1}^{S_i} \binom{S_i}{l_i}$$

$$\int_0^\infty \cdots \int_0^\infty \frac{(-1)^{l_i+1}}{\sum_{j\in\mathcal{K}} \lambda_j \left(\frac{P_j}{S_j}\right)^{\check{\alpha}} \mathbb{E}_{G_j^{\mathrm{ZF}}} \left[\left(\sum_{l_i'=1}^{l_i} G_{j,l_i'}^{\mathrm{ZF}} t_{l_i'} \right)^{\check{\alpha}} \right]} \prod_{l_i'=1}^{l_i} \bar{\mathcal{L}}_{\bar{\mathrm{F}}_{H_i^{\mathrm{ZF}}}}(t_{l_i'}) \mathrm{d}t_{l_i'} \tag{31}$$

$$\leq \frac{\pi}{\tilde{C}(\alpha)} \sum_{i\in\mathcal{K}} \sum_{l_i=1}^{S_i} \binom{S_i}{l_i} (-1)^{l_i+1} \frac{\frac{\lambda_i}{l_i^{\check{\alpha}}} \left(\frac{P_i}{S_i\beta_i}\right)^{\check{\alpha}} \left(\sum_{m_i=0}^{N^r-S_i} \frac{\Gamma(\frac{\check{\alpha}}{l_i}+m_i)}{\Gamma(\frac{\check{\alpha}}{l_i})\Gamma(1+m_i)} \right)^{l_i}}{\sum_{j\in\mathcal{K}} \lambda_j \left(\frac{P_j}{S_j}\right)^{\check{\alpha}} \left(\frac{\Gamma(\frac{\check{\alpha}}{l_i}+S_j)}{\Gamma(S_j)} \right)^{l_i}}. \tag{32}$$

Substituting (32) and (5) in (28) results in (11), completing the proof. □

REFERENCES

[1] D. Tse and P. Viswanath, *Fundamentals of Wireless Communication*. Cambridge University Press, September 2004.

[2] Q. Li *et al.*, "MIMO techniques in WiMAX and LTE: a feature overview," *IEEE Commun. Mag*, vol. 48, no. 5, pp. 86–92, May 2010.

[3] Cisco, "Visual networking index," Feb. 2014, white paper at Cisco.com.

[4] J. G. Andrews *et al.*, "What will 5G be?" *IEEE JSAC*, vol. 32, no. 6, pp. 1065–1082, Jun. 2014.

[5] ——, "Femtocells: Past, present, and future," *IEEE JSAC*, vol. 3, no. 3, pp. 497–508, Apr. 2012.

[6] D. Gesbert *et al.*, "Multi-cell mimo cooperative networks: A new look at interference," *IEEE JSAC*, vol. 28, no. 9, pp. 1380–1408, Dec. 2010.

[7] A. J. Goldsmith, *Wireless Communications*. Cambridge University Press, 2005.

[8] J. F. C. Kingman, *Poisson Processes*. Oxford University Press, 1993.

[9] M. Haenggi and R. K. Ganti, "Interference in large wireless networks," *Foundations and Trends in Networking*, vol. 3, no. 2, 2008, Available at http://www.nd.edu/ mhaenggi/pubs/now.pdf.

[10] E. S. Sousa and J. A. Silvester, "Optimum transmission ranges in a direct-sequence spread-spectrum multihop packet radio network," *IEEE JSAC*, vol. 8, no. 5, pp. 762–771, Jan. 1990.

[11] F. Baccelli *et al.*, "Stochastic analysis of spatial and opportunistic ALOHA," *IEEE JSAC*, vol. 27, no. 7, pp. 1105–1119, Sep. 2009.

[12] S. P. Weber *et al.*, "Transmission capacity of wireless ad hoc networks with successive interference cancellation," *IEEE Trans. on Inf. Theory*, vol. 53, no. 8, pp. 2799–2814, Aug. 2007.

[13] J. G. Andrews *et al.*, "A tractable approach to coverage and rate in cellular networks," *IEEE Trans. on Comm.*, vol. 59, no. 11, pp. 3122–3134, Nov. 2011.

[14] A. Guo and M. Haenggi, "Spatial stochastic models and metrics for the structure of base stations in cellular networks," *IEEE Trans. Wireless Comm.*, vol. 12, no. 11, pp. 5800–5812, Nov. 2013.

[15] O. Somekh *et al.*, "Sum rate characterization of joint multiple cell-site processing," *IEEE Trans. Inf. Theory*, vol. 53, no. 12, pp. 4473–4497, Dec. 2007.

[16] H. S. Dhillon *et al.*, "Modeling and analysis of K-tier downlink heterogeneous cellular network," *IEEE JSAC*, vol. 30, no. 3, pp. 550–560, Apr. 2012.

[17] S. Mukherjee, "Distribution on downlink SINR in heterogeneous cellular network," *IEEE JSAC*, vol. 30, no. 3, pp. 575–585, Apr. 2012.

[18] H. S. Jo *et al.*, "Heterogeneous cellular networks with flexible cell association: A compehensive downlink SINR analysis," *IEEE Trans. Wireless Comm.*, vol. 11, no. 10, pp. 3484–3495, Oct. 2012.

[19] P. Guan and M. D. Renzo, "Stochastic geometry analysis of the energy efficiency of downlink MIMO cellular networks," *in Proc. IEEE VTC Spring)*, pp. 1–5, 2015.

[20] R. H. Y. Louie *et al.*, "Open-loop spatial multiplexing and diversity communications in ad hoc networks," *IEEE Trans. Inf. Theory*, vol. 57, no. 1, pp. 317–344, Jan. 2011.

[21] R. Vaze and R. W. H. Jr., "Transmission capacity of ad-hoc networks with multiple antennas using transmit stream adaptation and interference cancellation," *IEEE Trans. Inf. Theory*, vol. 58, no. 2, pp. 780–792, Feb. 2012.

[22] A. Hunter *et al.*, "Transmission capacity of ad hoc networks with spatial diversity," *IEEE Trans. Wireless. Comm.*, vol. 7, no. 12, pp. 5058–5071, Dec. 2008.

[23] N. Jindal *et al.*, "Multi-antenna communication in ad hoc networks: Achieving MIMO gains with SIMO transmission," *IEEE Trans. on Comm.*, vol. 59, no. 2, pp. 529–540, Feb. 2011.

[24] N. Lee *et al.*, "Spectral efficiency scaling laws in dense random wireless networks with multiple receive antennas," *to appear in IEEE Trans. Inf. Theory*, 2016.

[25] V. Chandrasekhar *et al.*, "Coverage in multi-antenna two-tier networks," *IEEE Trans. Wireless. Comm.*, vol. 8, no. 10, pp. 5314–5327, Oct. 2009.

[26] H. S. Dhillon *et al.*, "Downlink MIMO hetnets: Modeling, ordering results and performance analysis," *IEEE Trans. Wireless. Comm.*, vol. 12, no. 10, pp. 5208–5222, Oct. 2013.

[27] M. Kountouris and J. G. Andrews, "Downlink sdma with limited feedback in interference-limited wireless networks," *IEEE Trans. Wireless. Comm.*, vol. 11, no. 8, pp. 2730–2741, Aug. 2012.

[28] C. Li *et al.*, "Analysis of area spectral efficiency and link reliability in multiuser MIMO HetNets," *in Proc. IEEE Int. Conf. Commun. (ICC)*, Jun. 2015.

[29] ——, "Success probability and area spectral efficiency in multiuser MIMO HetNets," *IEEE Trans. Comm.*, vol. 64, no. 4, pp. 1544–1556, Apr. 2016.

[30] A. K. Gupta *et al.*, "Downlink multi-antenna heterogeneous cellular network with load balancing," *IEEE Trans. Comm.*, vol. 62, no. 11, pp. 4052–4067, Nov. 2014.

[31] W. Lu and M. D. Renzo, "Stochastic geometry analysis of multi-user mimo cellular networks using zero-forcing precoding," *in Proc. IEEE Int. Conf. Commun. (ICC)*, pp. 1477–1482, Jun. 2015.

[32] R. Tanbourgi *et al.*, "Analysis of joint transmit-receive diversity in downlink MIMO heterogeneous cellular networks," *IEEE Trans. Wireless. Comm.*, vol. 14, no. 12, pp. 6695–6709, Jul. 2015.

[33] S. T. Veetil, "Performance of PZF and MMSE receivers in cellular networks with multi-user spatial multiplexing," *IEEE Trans. Wireless Comm.*, vol. 14, no. 9, pp. 4867–34 878, Sep. 2015.

[34] R. Tanbourgi *et al.*, "Dual-branch MRC receivers under spatial interference correlation and nakagami fading," *IEEE Trans. Comm.*, vol. 62, no. 6, pp. 1830–1844, Jun. 2014.

[35] U. Schilcher *et al.*, "Interference functionals in poisson networks," *IEEE Trans. Inf. Theory*, vol. 62, no. 1, pp. 370–383, Jan. 2016.

[36] Y. Lin *et al.*, "Optimizing user association and spectrum allocation in HetNets: A utility perspective," *IEEE JSAC*, vol. 33, no. 6, pp. 1025–1039, Jun. 2015.

[37] K. Huang *et al.*, "Spatial interference cancellation for multiantenna mobile ad hoc networks," *IEEE Trans. Inf. Theory*, vol. 58, no. 3, pp. 1660–1676, Mrc. 2012.

[38] M. Haenggi, "Diversity loss due to interference correlation," *IEEE Comm. Lett.*, vol. 16, no. 10, pp. 1600–1603, Oct. 2012.

[39] X. Zhang and J. G. Andrews, "Downlink cellular network analysis with multi-slope path loss models," *IEEE Trans. Comm.*, vol. 63, no. 5, pp. 1881–1894, May 2015.

[40] W. C. Ao *et al.*, "Bounds and exact mean node degree and node isolation probability in interference-limited wireless ad hoc networks with general fading," *IEEE TVT*, vol. 61, no. 5, pp. 2342–2348, Jun. 2012.

[41] M. Haenggi *et al.*, "Stochastic geometry and random graphs for the analysis and design of wireless networks," *IEEE JSAC*, vol. 27, no. 7, pp. 1029–1046, Sep. 2009.

[42] K. Hamdi, "Capacity of MRC on correlated Rician fading channels," *IEEE Trans. Comm.*, vol. 56, no. 5, pp. 708–711, May 2008.